Mon. Not. R. Astron. Soc. **388,** 1627–1651 (2008) doi:10.1111/j.1365-2966.2008.13224.x

Uncertainties in H_2 and HD chemistry and cooling and their role in early structure formation

S. C. O. Glover[1]★ and T. Abel[2]

[1]*Astrophysikalisches Institut Potsdam, An der Sternwarte 16, D-14482 Potsdam, Germany*
[2]*Kavli Institute for Particle Astrophysics and Cosmology, Stanford University, Menlo Park, CA 94025, USA*

Accepted 2008 March 12. Received 2008 March 12; in original form 2007 December 18

ABSTRACT

At low temperatures, the main coolant in primordial gas is molecular hydrogen, H_2. Recent work has shown that primordial gas that is not collapsing gravitationally but is cooling from an initially ionized state forms hydrogen deuteride, HD, in sufficient amounts to cool the gas to the temperature of the cosmic microwave background. This extra cooling can reduce the characteristic mass for gravitational fragmentation and may cause a shift in the characteristic masses of Population III stars. Motivated by the importance of the atomic and molecular data for the cosmological question, we assess several chemical and radiative processes that have hitherto been neglected: the sensitivity of the low-temperature H_2 cooling rate to the ratio of ortho-H_2 to para-H_2, the uncertainty in the low-temperature cooling rate of H_2 excited by collisions with atomic hydrogen, the effects of cooling from H_2 excited by collisions with protons and electrons, and the large uncertainties in the rates of several of the reactions responsible for determining the H_2 fraction in the gas.

It is shown that the most important of neglected processes is the excitation of H_2 by collisions with protons and electrons. Their effect is to cool the gas more rapidly at early times, and consequently to form less H_2 and HD at late times. This fact, as well as several of the chemical uncertainties presented here, significantly affects the thermal evolution of the gas. We anticipate that this may lead to clear differences in future detailed three-dimensional studies of first structure formation. In such calculations it has previously been shown that the details of the timing between cooling and merger events decide between immediate runaway gravitational collapse and a slower collapse delayed by turbulent heating.

Finally, we show that although the thermal evolution of the gas is in principle sensitive to the ortho–para ratio, in practice the standard assumption of a 3:1 ratio produces results that are almost indistinguishable from those produced by a more detailed treatment.

Key words: molecular data – molecular processes – stars: formation – cosmology: theory.

1 INTRODUCTION

The very first stars to form in the Universe are believed to have formed within small protogalactic objects, cooled primarily by molecular hydrogen (H_2). Molecular hydrogen cooling becomes ineffective at temperatures below $T \lesssim 200\,\mathrm{K}$, and at gas number densities $n > 10^4\,\mathrm{cm}^{-3}$, and so any dense fragments that form in the cooling and collapsing gas have a characteristic mass of a few hundred solar masses, set by the Jeans mass at this temperature and density (Abel, Bryan & Norman 2002; Bromm, Coppi & Larson 2002; see also the reviews of Bromm & Larson 2004; Glover 2005). Since there is little evidence for subfragmentation during later stages of the collapse (although for a dissenting view see Clark, Glover & Klessen 2008), and since the high gas temperature leads to a high protostellar accretion rate, there seems little to limit the growth of the first stars, which may easily grow to $\sim 100\,\mathrm{M}_\odot$ or more (see e.g. Yoshida et al. 2006; O'Shea & Norman 2007).

Efficient cooling from hydrogen deuteride, HD, can alter this scenario. HD can cool the gas to lower temperatures than H_2, and remains an effective coolant up to higher densities, $n \sim 10^6\,\mathrm{cm}^{-3}$. The characteristic mass of stars formed in HD-cooled gas is therefore believed to be smaller, $\sim 10\,\mathrm{M}_\odot$ (Johnson & Bromm 2006; Yoshida et al. 2007), reflecting the smaller characteristic mass scale imprinted on the cooling gas. However, HD cooling will only bring about a change of this kind in the characteristic mass scale if enough forms to cool the gas efficiently. Bromm et al. (2002) show that in simulations following the formation of the very first stars, in protogalaxies with virial temperatures $T_{\mathrm{vir}} < 10^4\,\mathrm{K}$, this does not occur: the inclusion of deuterium chemistry and HD cooling has

★E-mail: sglover@aip.de

very little effect on the outcome. On the other hand, various authors have shown that in gas cooling from an initially ionized state, enough HD forms to cool the gas down to temperatures close to the temperature of the cosmic microwave background (CMB) (Nakamura & Umemura 2002; Nagakura & Omukai 2005; Johnson & Bromm 2006; Shchekinov & Vasiliev 2006; Johnson, Greif & Bromm 2007; Yoshida et al. 2007). Note, however, that even without HD cooling the characteristic masses of objects collapsing from gas within a relic primordial H II region have already been demonstrated to be smaller (O'Shea et al. 2005).

This difference in thermal evolution, depending on whether or not the gas was once ionized, is a consequence of the chemistry of HD formation and destruction. The dominant reactions regulating the amount of HD in the gas are

$$H_2 + D^+ \rightarrow HD + H^+ \quad (1)$$

and

$$HD + H^+ \rightarrow H_2 + D^+. \quad (2)$$

Reaction (1) is exothermic, while reaction (2) is endothermic by 0.0398 eV (462 K), and so at low temperatures, chemical fractionation occurs: the HD:H_2 ratio becomes enhanced over the cosmological D:H ratio by a large numerical factor. Consequently, even though the HD cooling rate per molecule decreases with decreasing temperature, the HD cooling rate per unit volume can actually increase, owing to the increase in the HD abundance produced by this fractionation process (see e.g. Glover 2008). In conventional Population III star formation calculations (e.g. Abel et al. 2002), the fractional ionization is small, and because of $p\,\mathrm{d}V$ heating the gas temperature never becomes low enough for chemical fractionation to become efficient. Therefore, HD cooling remains unimportant. In contrast, in gas cooling from an initially ionized state, more H_2 forms, owing to the non-equilibrium fractional ionization in the cooling gas (Shapiro & Kang 1987), and the gas can reach a lower temperature. In practice, the extra cooling provided by the enhanced H_2 abundance is sufficient to cool the gas to a point at which chemical fractionation becomes very important, following which HD dominates the cooling.

Several processes and rate uncertainties, hitherto neglected, may interfere with this simple picture. First, most calculations assume a ratio of ortho-hydrogen (H_2 with nuclear spin quantum number $I = 1$) to para-hydrogen (H_2 with $I = 0$) that is $(2I_{\mathrm{ortho}} + 1)/(2I_{\mathrm{para}} + 1) = 3$. This value is appropriate for warm H_2 in local thermodynamic equilibrium (LTE), which has many different rotational and vibrational levels populated, but at low temperatures and low densities, the ortho–para ratio may differ significantly from this value. For instance, if only the $J = 0$ and 1 rotational levels of the vibrational ground state are populated, then the equilibrium ortho–para ratio is $9\exp(-170.5/T)$. The relevance of this to the current situation lies in the fact that the energy associated with the $v = 0, J = 2 \rightarrow 0$ rotational transition in para-hydrogen, $E_{20} = 509.85$ K, is significantly smaller than the energy associated with the $v = 0, J = 3 \rightarrow 1$ transition in ortho-hydrogen, $E_{31} = 844.65$ K. Consequently, para-hydrogen can cool the gas to lower temperatures than ortho-hydrogen. It is therefore possible that the ability of the gas to cool to the low temperatures required for HD cooling to take over and dominate will be sensitive to the assumed ortho–para ratio, and that the outcome of calculations that determine it accurately will differ from that of calculations that assume a ratio of 3:1.

A second issue affecting existing calculations is the fact that the low-temperature behaviour of the H_2 cooling rate remains uncertain. The root cause of this uncertainty is the sensitivity of the low-energy H–H_2 excitation cross-sections to the choice of the interaction potential used to calculate them. Most previous studies of HD cooling in primordial gas have made use of the fit to the low-density H_2 cooling rate given by Galli & Palla (1998). At $T < 600$ K, this fit is based on excitation rates from Forrey et al. (1997) that were calculated using the BKMP2 potential energy surface of Boothroyd et al. (1996). However, recently Wrathmall & Flower (2007) have published a new set of H_2 collisional excitation rate coefficients based on calculations performed using the Mielke, Garrett & Peterson (2002) potential energy surface. The H_2 cooling function derived from these revised excitation rates differs significantly from the Galli & Palla (1998) rate at temperatures $T < 1000$ K, but the consequences of this reduction in the cooling rate have yet to be explored in much detail.

A third issue regarding the H_2 cooling rate is that fact that most previous calculations have only included the effects of collisional excitation of H_2 by atomic hydrogen. However, H_2 can also be excited by collisions with H_2, He, H^+ and e^-. As we show in Section 3.2, in the conditions of interest for HD formation, several of these neglected processes play important roles.

The final issue affecting studies of the role of HD cooling that we examine here is the impact of the large uncertainties that exist in several key rate coefficients for chemical reactions involved in the formation and destruction of H_2. Although some of these uncertainties (which are discussed in detail in Section 2.1) have received previous study in the literature (Savin et al. 2004; Glover, Savin & Jappsen 2006), their impact on the ability of the gas to cool to temperatures at which HD cooling becomes dominant has not previously been explored.

In this paper, we explore these issues with the aid of a detailed chemical and thermal model of primordial gas, coupled to two simple dynamical models. Our main aim is to determine whether any of these sources of uncertainty can plausibly lead to significant differences in the evolution of the gas, or whether existing results on the role of HD cooling are robust. The structure of this paper is as follows. In Section 2, we outline the numerical model used in this work. In this context, we also discuss in more detail the major uncertainties highlighted above. In Section 3, we present and discuss our results, and we conclude in Section 4 with a brief summary.

2 NUMERICAL MODEL

2.1 Chemical network

To model the chemistry of H_2 and HD in primordial gas, we use a chemical network consisting of 115 reactions between 16 species, as summarized in Table A1. This network differs significantly from previous treatments of primordial deuterium chemistry in that it includes the formation and destruction of doubly deuterated hydrogen, D_2. This is included because it has been suggested (D. Savin, private communication) that conversion of HD to D_2 at low gas temperatures may be a significant destruction mechanism for HD, although in practice we find that it is unimportant.

For simplicity, we omit H_3^+, HeH^+ and their deuterated analogues from our chemical model. The abundances of these species are very small and their influence on the cooling of the gas at intermediate to low densities is minimal (Glover & Savin 2006; Glover & Savin, in preparation), so their omission should not significantly affect our results. We also omit lithium, for similar reasons.

We assume that any radiation backgrounds are negligible and so do not include any processes involving photoionization or photodissociation. We also neglect cosmic ray ionization; the

influence of this latter process on promoting HD cooling has been treated in detail elsewhere (Shchekinov & Vasiliev 2004; Vasiliev & Shchekinov 2006; Jasche, Ciardi & Ensslin 2007; Stacy & Bromm 2007).

Whenever possible, rates for deuterated analogues of the basic hydrogen reactions have been taken from the primary literature, or from the compilations of Stancil, Lepp & Dalgarno (1998), Wang & Stancil (2002) and Walmsley, Flower & Pineau des Forêts (2004). However, some reactions do not appear to have been previously considered in the astrochemical literature. In cases where we have been unable to find an appropriate rate, we have generally adopted the same procedure as in Stancil et al. (1998): for a non-deuterated reaction with a reaction rate that has a power-law temperature dependence $k \propto T^m$, we have generated the rates of the deuterated analogues by multiplying this rate by a scaling factor $(\mu_{\rm H}/\mu_{\rm D})^m$, where $\mu_{\rm H}$ and $\mu_{\rm D}$ are the reduced masses of the reactants in the non-deuterated and deuterated reactions, respectively.

For reactions where the presence of a deuteron increases the number of distinguishable outcomes – e.g. the dissociative attachment of HD with e^- (reactions 57–58), which can produce either H and D^- or H^- and D, in contrast to the dissociative attachment of H_2 with e^- (reaction 23) which can only produce H^- and H – and where no good information exists on the branching ratio of the reaction, we assume that the probability of each outcome is uniform. For this particular example, this gives branching ratios of 50 per cent for reactions (57) and (58), respectively.

Finally, the rate coefficients for several of the included reactions require more detailed discussion, which can be found in Sections 2.1.1–2.1.7 below.

2.1.1 Associative detachment and mutual neutralization of H^- and D^-

The rates of reactions (2) and (5), i.e. the associative detachment of H^- with H,

$$H^- + H \rightarrow H_2 + e^-, \tag{3}$$

and the mutual neutralization of H^- with H^+,

$$H^- + H^+ \rightarrow H + H, \tag{4}$$

are uncertain by up to an order of magnitude. When the fractional ionization of the gas is small, these uncertainties are unimportant, as in this case reaction (2) proceeds much faster than reaction (5). However, in gas with a high fractional ionization, such as gas recombining from an initially ionized state, reaction (5) competes with reaction (2) for the available H^- ions and so the uncertainties in the rates of these reactions introduce a significant uncertainty into the amount of H_2 that is formed. A large associative detachment rate and small mutual neutralization rate lead to the production of a larger H_2 fraction (at a given time) than a small associative detachment rate and large mutual neutralization rate (Glover et al. 2006).

The default value for k_2 in our models is

$$k_2 = 1.3 \times 10^{-9}\,{\rm cm^3\,s^{-1}}, \tag{5}$$

based on the measurement of Schmeltekopf, Fehsenfeld & Ferguson (1967). However, in Section 3.3 we present results from models performed using

$$k_2 = 5.0 \times 10^{-9}\,{\rm cm^3\,s^{-1}} \tag{6}$$

and

$$k_2 = 0.65 \times 10^{-9}\,{\rm cm^3\,s^{-1}}, \tag{7}$$

which represent plausible upper and lower bounds on the actual rate (Glover et al. 2006).

Similarly, our default value for k_5 is given by

$$k_5 = 2.4 \times 10^{-6} T^{-0.5} \left(1.0 + \frac{T}{20\,000}\right)\,{\rm cm^3\,s^{-1}}, \tag{8}$$

taken from Croft, Dickinson & Gadea (1999), but in Section 3.3 we also examine models using

$$k_5 = 5.7 \times 10^{-6} T^{-0.5} + 6.3 \times 10^{-8} - 9.2 \times 10^{-11} T^{0.5} + 4.4 \times 10^{-13} T\,{\rm cm^3\,s^{-1}}, \tag{9}$$

taken from Moseley, Aberth & Peterson (1970) and

$$k_5 = 7.0 \times 10^{-7} T^{-0.5}\,{\rm cm^3\,s^{-1}}, \tag{10}$$

taken from Dalgarno & Lepp (1987). Glover et al. (2006) have suggested that the last of these rates may be erroneously small, owing to typographical errors in Dalgarno & Lepp (1987). Nevertheless, this rate has been used in a number of recent models of HD formation in primordial gas (see e.g. Nagakura & Omukai 2005; Johnson & Bromm 2006), justifying its consideration here.

In view of the large uncertainties in the rates of reactions (2) and (5), we have assumed that identical rates apply for the deuterated analogues of these reactions (numbers 54–56 and 66–68), since any small differences in the basic rates caused by the presence of one or two deuterons in place of protons are likely swamped by this basic uncertainty.

2.1.2 Charge transfer from H^+ to H_2 (reaction 7)

The most accurate cross-section for this process at astrophysically relevant energies is that computed by Krstić (2002); the corresponding thermal rate coefficient is given in Savin et al. (2004). However, as Savin et al. (2004) discuss in some detail, a large number of other rates for this reaction are given in the literature, differing by orders of magnitude at temperatures below 10^4 K. As this reaction is an important H_2 destruction mechanism, particularly in gas recombining from an initially ionized state, and as most previous studies of HD formation in primordial gas have used one or another of these less accurate rate coefficients (Yoshida et al. 2007 are a notable exception), it seems appropriate to examine the effect that the choice of this rate coefficient has on the final amount of H_2 formed and on the ability of the gas to cool to temperatures at which HD cooling becomes dominant. Therefore, while we use the Savin et al. (2004) rate in most of our models, we examine in Section 3.3 the effect of using two other rates from the literature.

The first of these, from Shapiro & Kang (1987),

$$k_7 = 2.4 \times 10^{-9} \exp\left(-\frac{21\,200}{T}\right)\,{\rm cm^3\,s^{-1}}, \tag{11}$$

is, strictly speaking, only applicable to vibrationally excited H_2, but in spite of this Johnson & Bromm (2006) use this rate for charge transfer with ground-state H_2 in their study of HD cooling. As the comparison in fig. 1 of Savin et al. (2004) demonstrates, this rate is significantly larger than other determinations in the literature.

At the other extreme, Abel et al. (1997) quote a rate

$$\begin{aligned} k_7 = \exp(&-24.249\,1469 \\ &+ 3.400\,8244(\ln T_e) \\ &- 3.898\,0040(\ln T_e)^2 \\ &+ 2.045\,5878(\ln T_e)^3 \\ &- 5.416\,1829 \times 10^{-1}(\ln T_e)^4 \\ &+ 8.410\,7750 \times 10^{-2}(\ln T_e)^5 \\ &- 7.879\,0262 \times 10^{-3}(\ln T_e)^6 \\ &+ 4.138\,3984 \times 10^{-4}(\ln T_e)^7 \\ &- 9.363\,4588 \times 10^{-6}(\ln T_e)^8\big)\ \mathrm{cm^3\ s^{-1}}, \end{aligned} \quad (12)$$

where T_e is the gas temperature in units of eV. This rate is based on Janev et al. (1987), and has subsequently been adopted by a number of authors (see e.g. Nagakura & Omukai 2005). However, it is much smaller at $T < 10^4$ K than any of the other determinations in the Savin et al. (2004) comparison.

2.1.3 Collisional dissociation of H_2 (reactions 8–11)

In Table A1, we list two rates for each process: one for H_2 that is all in the vibrational ground state (appropriate for low-density gas), and one for H_2 with LTE level populations. At intermediate densities, we adopt a rate coefficient for each reaction given by

$$\log k_i = \left(\frac{n/n_{\rm cr}}{1 + n/n_{\rm cr}}\right) \log k_{\rm i,LTE} + \left(\frac{1}{1 + n/n_{\rm cr}}\right) \log k_{\rm i,v=0}, \quad (13)$$

where k_i is the collisional dissociation rate for collisions with species i, $k_{\rm v=0,i}$ and $k_{\rm LTE,i}$ are the rates for this reaction in the $v = 0$ and LTE limits, respectively, and $n_{\rm cr}$ is the critical density, given by

$$\frac{1}{n_{\rm cr}} = \frac{x_{\rm H}}{n_{\rm cr,H}} + \frac{x_{\rm H_2}}{n_{\rm cr,H_2}} + \frac{x_{\rm He}}{n_{\rm cr,He}}. \quad (14)$$

Here, $x_{\rm H} = n_{\rm H}/n$, $x_{\rm H_2} = 2n_{\rm H_2}/n$, $x_{\rm He} = n_{\rm He}/n$, n is the number density of hydrogen nuclei, and

$$n_{\rm cr,H} = \mathrm{dex}\left[3.0 - 0.416 \log T_4 - 0.327\,(\log T_4)^2\right], \quad (15)$$

$$n_{\rm cr,H_2} = \mathrm{dex}\left[4.845 - 1.3 \log T_4 + 1.62\,(\log T_4)^2\right] \quad (16)$$

and

$$n_{\rm cr,He} = \mathrm{dex}[5.0792\{1.0 - 1.23 \times 10^{-5}(T - 2000)\}], \quad (17)$$

with $T_4 = T/10\,000$ K. The expression for $n_{\rm cr,H}$ is from Lepp & Shull (1983), but has been decreased by an order of magnitude, as recommended by Martin, Schwarz & Mandy (1996). The expression for $n_{\rm cr,H_2}$ comes from Shapiro & Kang (1987), and the expression for $n_{\rm cr,He}$ comes from Dove et al. (1987). Note that this expression for the critical density assumes that in high-density gas, $n_e \ll n_{\rm H}$, so that electron excitation of H_2 does not significantly affect the value of $n_{\rm cr}$.

2.1.4 He^+ recombination (reaction 19)

In optically thick gas that is a mixture of neutral H and He, the effective He^+ recombination coefficient is given by

$$k_{19} = 0.68k_{19,\rm rr,A} + 0.32k_{19,\rm rr,B} + k_{19,\rm di}, \quad (18)$$

where we have assumed that $n_{\rm H_2} \ll n_{\rm H}$; see Osterbrock (1989) for a more detailed discussion.

In these conditions, it is also necessary to take account of the photoionization of H caused by the He^+ recombination emission. As long as the gas is highly optically thick above the Lyman limit, this can be modelled as a local H ionization rate with a value

$$R_{\rm pi} = k_{\rm pi} n_e n_{\rm He^+}\ \mathrm{cm^{-3}\ s^{-1}}, \quad (19)$$

where

$$k_{\rm pi} = [0.68k_{19,\rm rr,A} + 0.28k_{19,\rm rr,B} + 2k_{19,\rm di}]. \quad (20)$$

We have not included a similar contribution from He^{++} recombination, as in conditions where the He^{++} abundance is significant, we expect H to be almost completely ionized.

2.1.5 Three-body H_2 formation (reactions 30 and 31)

At high densities, reactions (30) and (31) are important sources of H_2. However, the rate coefficients for these reactions are highly uncertain, as previously discussed in Glover (2008). To assess the importance of this uncertainty on our results, we have carried out simulations using two different values for k_{30}: the first, taken from Abel et al. (2002) and partially based on Orel (1987) is the lowest of the values we have found in the literature:

$$k_{30} = \begin{cases} 1.14 \times 10^{-31} T^{-0.38}\ \mathrm{cm^3\ s^{-1}} & T \leqslant 300\,\mathrm{K}, \\ 3.9 \times 10^{-30} T^{-1.0}\ \mathrm{cm^3\ s^{-1}} & T > 300\,\mathrm{K}. \end{cases} \quad (21)$$

The other, taken from the recent paper of Flower & Harris (2007) has the highest value at low temperatures of any of the rates we have found

$$k_{30} = 1.44 \times 10^{-26} T^{-1.54}\ \mathrm{cm^3\ s^{-1}}. \quad (22)$$

To fix the rate of reaction (31), we follow Palla, Salpeter & Stahler (1983) and assume that $k_{31} = k_{30}/8$.

2.1.6 Destruction of D_2 by collision with H (reaction 107)

The data tabulated in Mielke et al. (2003) span the temperature range $200 \leqslant T \leqslant 2200$ K. At lower temperatures, we simply extrapolate our fit to the higher temperature data: this fit remains well behaved at low temperatures; and since the rate of this reaction falls off exponentially at low T, we are not particularly sensitive to errors in its value in this temperature range. At $T > 2200$ K, we use the simple exponential fit given by Mielke et al. (2003) to their high-temperature calculations; although not formally valid at these temperatures, the fit remains well behaved, and hopefully lies not too far from the true value.

2.1.7 Collisional dissociation of HD and D_2 (reactions 108–115)

For collisions with electrons, accurate rates are available in Trevisan & Tennyson (2002a) and Trevisan & Tennyson (2002b). For collisions with H, H_2 or He, however, we have been unable to find a treatment in the literature. We have therefore assumed that the rates of these reactions in the $v = 0$ and LTE limits are the same as for the corresponding H reactions (numbers 8–10). For D_2, we also adopt the same value for the critical density, while for HD, we increase $n_{\rm cr}$ by a factor of 100 to account for its larger radiative transition probabilities. Note that although these rates are highly approximate, this probably does not introduce much uncertainty into the chemical model, as reactions (40) and (107) become effective at much lower temperatures and therefore will generally dominate the destruction of HD and D_2 in warm gas.

2.2 The ortho–para hydrogen ratio

In order to follow the evolution of the ortho–para hydrogen ratio in the gas, we directly follow the time-dependent level populations of the lowest four energy levels of the H_2 molecule, the $J = 0, 1, 2$ and 3 rotational levels of the vibrational ground state. Rates for collisional transitions between these four states are taken from several sources: non-reactive collisions with H (which cannot change the ortho–para ratio) are treated using the rates computed by Wrathmall & Flower (2007), while for reactive collisions (which *can* change the ortho–para ratio), we use the rates suggested by Le Bourlot, Pineau des Forêts & Flower (1999). Collisions with protons are treated using the rates computed by Gerlich (1990). Radiative transitions rates are taken from Wolniewicz, Simbotin & Dalgarno (1998).

Newly formed H_2 is assumed, for simplicity, to reside in the $J = 0$ ground state. This assumption is not correct: H_2 formed by associative detachment of H^- is, in general, highly excited and has a non-zero ortho–para ratio (Launay, Le Dourneuf & Zeippen 1991). However, it is easy to show that this assumption has little effect on the ortho–para ratio. In conditions where associative detachment dominates the destruction of H^-, we can write the H_2 formation time-scale as

$$t_{\rm form} = \frac{x_{\rm H_2}}{k_1 x_{\rm e^-} n}, \tag{23}$$

where $x_{\rm H_2}$ and $x_{\rm e^-}$ are the fractional abundances of H_2 and free electrons, respectively. In comparison, collisions with protons cause the ortho–para ratio to reach equilibrium on a time-scale

$$t_{\rm op} = \frac{f_{\rm op}}{k_{\rm op} x_{\rm H^+} n}, \tag{24}$$

where $f_{\rm op}$ is the ortho–para ratio, $x_{\rm H^+}$ is the fractional abundance of protons, and $k_{\rm op}$ is an appropriately averaged rate coefficient for the conversion of ortho-H_2 to para-H_2 by proton collision. From Gerlich (1990), we know that $k_{\rm op} \sim 10^{-10}\,{\rm cm^3\,s^{-1}}$, while from Table A1 we see that at a representative low temperature of 200 K, $k_1 = 2.07 \times 10^{-16}\,{\rm cm^3\,s^{-1}}$. Thus, the time-scales are comparable only if

$$x_{\rm H_2} \sim 10^{-6} f_{\rm op} \frac{x_{\rm e^-}}{x_{\rm H^+}}. \tag{25}$$

If we make the reasonable assumption that $x_{\rm e^-} \simeq x_{\rm H^+}$, and that $f_{\rm op}$ is of the order of unity, then this argument demonstrates that the H_2 formation process has a significant effect on the ortho–para ratio only when the H_2 fraction is very small, $x_{\rm H_2} \lesssim 10^{-6}$.

A similar comparison can also be performed between the H_2 formation time-scale and the lifetimes of excited states of H_2, but again the aftereffects of the formation process are important only when the H_2 fraction is very small.

Our model for the ortho–para ratio becomes increasingly inaccurate at high temperatures, as the excitation of states with $J > 3$ or $v > 0$ becomes important, but since the sensitivity of the H_2 cooling rate to the ortho–para ratio is large only at low temperatures (see Section 2.3 below), this simplified approach is sufficient for our purposes.

2.3 Thermal processes

2.3.1 H_2 cooling: collisions with H

As we have already discussed in Section 1, the low-temperature rates for the collisional excitation of H_2 by H are highly sensitive to the choice of potential energy surface used to describe the H_3 system (Sun & Dalgarno 1994). An accurate determination of the H_2 cooling function at low temperatures and low gas densities requires a level of accuracy in the potential that has been difficult to achieve, and as a consequence there are a number of determinations of the low-density limit of the H_2 cooling function in the literature that differ substantially at temperatures $T < 1000\,{\rm K}$ (see e.g. the comparison in fig. A1 of Galli & Palla 1998). In recent years, the most widely used version has been that of Galli & Palla (1998):[1]

$$\Lambda_{\rm H_2,GP} = {\rm dex}[-103.0 + 97.59 \log T - 48.05 (\log T)^2 + 10.80 (\log T)^3 - 0.9032 (\log T)^4]. \tag{26}$$

This rate is based on two separate sets of collisional rate coefficients. At temperatures $T < 600\,{\rm K}$, the rates used are those computed by Forrey et al. (1997) using a fully quantal approach and the BKMP2 potential energy surface of Boothroyd et al. (1996). At $T > 600\,{\rm K}$, the rates used are those of Mandy & Martin (1993), which were computed using the quasi-classical trajectory approach and the Liu–Siegbahn–Truhlar–Horowitz potential energy surface (Liu 1973; Siegbahn & Liu 1978; Truhlar & Horowitz 1978). An ortho–para ratio of 3:1 is assumed at all temperatures.

Recently, however, Wrathmall & Flower (2007) have published a new set of collisional rate coefficients computed using the potential energy surface of Mielke et al. (2002). The rms error in this new potential energy surface is more than an order of magnitude smaller than the error in the Boothroyd et al. (1996) potential, and Wrathmall & Flower (2007) argue that it should allow a more accurate determination of the near-threshold behaviour of H_2, and hence a better determination of the low-temperature excitation rates and cooling rate. Wrathmall & Flower (2007) and Wrathmall, Gusdorf & Flower (2007) show that there are indeed significant differences in the low-temperature behaviour of a number of different excitation rates.

We have used the rate coefficients calculated by Wrathmall & Flower (2007) to compute separate cooling rates for ortho-H_2 and para-H_2 in the low-density limit due to collisions with atomic hydrogen. For ortho-H_2, we find that the cooling rate in the temperature range $100 < T < 6000\,{\rm K}$ is fitted to within 2 per cent with a function of the form

$$\log \Lambda_{\rm H_2,H} = \sum_{i=0}^{7} a_i \log(T_3)^i, \tag{27}$$

where $T_3 = T/1000\,{\rm K}$. The fitting coefficients a_i are listed in Table 1. Below 100 K, we extrapolate the Wrathmall & Flower (2007) rate as

$$\Lambda_{\rm oH_2,H} = 5.09 \times 10^{-27} T_3^{1/2} \exp\left(\frac{-852.5}{T}\right). \tag{28}$$

Table 1. Fitting coefficients for the cooling rate of ortho-H_2 excited by collisions with atomic hydrogen.

Coefficient	$100 < T < 1000\,{\rm K}$	$1000 \leqslant T < 6000\,{\rm K}$
a_0	−24.330 855	−24.329 086
a_1	4.440 4496	4.610 5087
a_2	−4.046 0989	−3.950 5350
a_3	−1.139 0725	12.363 818
a_4	9.809 4223	−32.403 165
a_5	8.627 3872	48.853 562
a_6	0.0	−38.542 008
a_7	0.0	12.066 770

[1] This cooling rate has units of erg cm^3 s^{-1}, as do all of the other cooling rates quoted in this paper, unless indicated otherwise.

Table 2. Fitting coefficients for the cooling rate of para-H_2 excited by collisions with atomic hydrogen.

Coefficient	$100 < T < 1000$ K	$1000 \leqslant T < 6000$ K
a_0	−24.216 387	−24.216 387
a_1	3.323 7480	4.204 6488
a_2	−11.642 384	−1.315 5285
a_3	−35.553 366	−1.655 2763
a_4	−35.105 689	4.178 0102
a_5	−10.922 078	−0.569 496 97
a_6	0.0	−3.382 4407
a_7	0.0	1.090 4027

Note that as HD cooling dominates at these low temperatures, we are not particularly sensitive to errors in this extrapolation.

For para-H_2, we follow a similar procedure: the para-H_2 cooling rate for $100 < T < 6000$ K can again be fitted to within 3 per cent by a function of the form of equation (27), using the fitting coefficients listed in Table 2. At $T < 100$ K, we use the extrapolation

$$\Lambda_{\mathrm{pH_2,H}} = 8.16 \times 10^{-26} T_3^{1/2} \exp\left(\frac{-509.85}{T}\right). \quad (29)$$

Given these partial rates, the total H_2 cooling rate in the low-density limit due to collisions with atomic hydrogen for gas with an ortho-hydrogen abundance x_o and para-hydrogen abundance x_p is then simply

$$\Lambda_{\mathrm{H_2,H}} = \left(\frac{x_\mathrm{o}}{x_\mathrm{o}+x_\mathrm{p}}\right)\Lambda_{\mathrm{oH_2,H}} + \left(\frac{x_\mathrm{p}}{x_\mathrm{o}+x_\mathrm{p}}\right)\Lambda_{\mathrm{pH_2,H}}. \quad (30)$$

2.3.2 H_2 cooling: collisions with H_2

To treat cooling due to collisions between two H_2 molecules, we follow Flower et al. (2000a) and use rates for the excitation of para-H_2 and ortho-H_2 by ground-state para-H_2 derived from Flower & Roueff (1998) and rates for the excitation of para-H_2 and ortho-H_2 by ground-state ortho-H_2 derived from Flower & Roueff (1999). In the low-density limit, and for temperatures in the range $100 < T < 6000$ K, these rates are fitted to within 2 per cent by functions of the form

$$\log \Lambda_{\mathrm{H_2,H_2}} = \sum_{i=0}^{5} a_i \log(T_3)^i. \quad (31)$$

The fitting coefficients are listed in Tables 3 and 4 for cooling from para-H_2 and ortho-H_2, respectively.

The total cooling rate in gas with an ortho-H_2 abundance x_o and a para-H_2 abundance x_p is given by

$$\Lambda_{\mathrm{H_2,H_2}} = x_\mathrm{p}^2 \Lambda_{\mathrm{pH_2,pH_2}} + x_\mathrm{p} x_\mathrm{o} \Lambda_{\mathrm{pH_2,oH_2}} + x_\mathrm{o} x_\mathrm{p} \Lambda_{\mathrm{oH_2,pH_2}} + x_\mathrm{o}^2 \Lambda_{\mathrm{oH_2,oH_2}}, \quad (32)$$

Table 3. Fitting coefficients for the cooling rate of para-H_2 excited by collisions with H_2.

Coefficient	Para-H_2	Ortho-H_2
a_0	−23.889 798	−23.748 534
a_1	1.855 0774	1.766 764 80
a_2	−0.555 933 88	−0.586 343 25
a_3	0.284 293 61	0.310 741 59
a_4	−0.205 811 13	−0.174 556 29
a_5	0.131 123 78	0.185 307 58

Table 4. Fitting coefficients for the cooling rate of ortho-H_2 excited by collisions with H_2.

Coefficient	Para-H_2	Ortho-H_2
a_0	−24.126 177	−24.020 047
a_1	2.325 8217	2.268 7566
a_2	−1.008 2491	−1.020 0304
a_3	0.548 237 68	0.835 614 32
a_4	−0.336 797 59	−0.407 722 47
a_5	0.207 714 06	0.096 025 713

where $\Lambda_{\mathrm{pH_2,pH_2}}$ denotes the cooling rate due to the excitation of para-H_2 by para-H_2, $\Lambda_{\mathrm{pH_2,oH_2}}$ the cooling rate due to the excitation of para-H_2 by ortho-H_2, etc.

2.3.3 H_2 cooling: collisions with He

The excitation of H_2 by collisions with helium has been studied by a large number of authors (see e.g. Lee et al. 2005, and references therein). Currently, the most reliable theoretical calculations appear to be those performed using the Muchnick & Russek (1994) HeH_2 potential energy surface (e.g. Flower, Roueff & Zeippen 1998; Balakrishnan, Forrey & Dalgarno 1999a; Balakrishnan et al. 1999b). The more recent Boothroyd, Martin & Peterson (2003) surface, which was expected to be more accurate, produces results for some transitions that are in serious conflict with experimental determinations (Lee et al. 2005) and so results derived using this potential energy surface are currently not considered reliable.

In our models, we use an H_2 cooling rate due to collisions with He that is derived from the calculations of Flower et al. (1998) for temperatures in the range $100 < T < 6000$ K and from Balakrishnan et al. (1999a) for temperatures $T < 100$ K (which were not treated in the Flower et al. study). Comparison of the Flower et al. (1998) and Balakrishnan et al. (1999a) rates at temperatures $T > 100$ K shows that they agree to within 10 per cent. As before, we have derived separate rates for ortho-H_2 and para-H_2. In the low-density limit, both cooling rates are fitted to within 1 per cent for temperatures $T < 6000$ K by a function of the form

$$\log \Lambda_{\mathrm{H_2,He}} = \sum_{i=0}^{5} a_i \log(T_3)^i, \quad (33)$$

where $T_3 = T/1000$ K. The fitting coefficients a_i for the ortho and para cases are listed in Table 5.

2.3.4 H_2 cooling: collisions with protons and electrons

In gas with a significant fractional ionization, collisions with protons and electrons can lead to a substantial H_2 cooling rate. To treat the

Table 5. Fitting coefficients for the cooling rate of H_2 excited by collisions with atomic helium.

Coefficient	Para-H_2	Ortho-H_2
a_0	−23.489 029	−23.7749
a_1	1.821 0825	2.406 54
a_2	−0.591 105 59	−1.234 49
a_3	0.422 806 23	0.739 874
a_4	−0.301 711 38	−0.258 940
a_5	0.128 728 39	0.120 573

Table 6. Fitting coefficients for the cooling rate of H_2 excited by collisions with protons.

Coefficient	Para-H_2	Ortho-H_2
a_0	−21.757 160	−21.706 641
a_1	1.399 8367	1.390 1283
a_2	−0.372 095 30	−0.349 936 99
a_3	0.061 554 519	0.075 402 398
a_4	−0.372 382 86	−0.231 707 23
a_5	0.233 141 57	0.068 938 876

Table 7. Fitting coefficients for the cooling rate of H_2 excited by collisions with electrons.

Coefficient	Para-H_2 $T \leqslant 10^3$ K	Para-H_2 $T > 10^3$ K	Ortho-H_2
a_0	−22.817 869	−22.817 869	−21.703 215
a_1	0.956 534 74	0.669 161 41	0.760 595 65
a_2	0.792 834 62	7.119 1428	0.506 448 90
a_3	0.568 117 79	−11.176 835	0.050 371 349
a_4	0.278 950 33	7.046 7275	−0.103 724 67
a_5	0.056 049 813	−1.647 1816	−0.035 709 409

effect of collisions with protons, we use the rotational excitation rates of Gerlich (1990) and the vibrational cross-sections of Krstić (2002). In the low-density limit, the cooling rates of ortho-H_2 and para-H_2 due to pure rotational transitions to levels with $2 \leqslant J \leqslant 7$ in the vibrational ground state, plus pure vibrational transitions to levels with $1 \leqslant v \leqslant 4$ can be fitted to within 2 per cent over the temperature range $10 < T < 10\,000$ K by a function of the form

$$\log \Lambda_{\mathrm{H_2,H^+}} = \sum_{i=0}^{5} a_i \log(T_3)^i, \tag{34}$$

where $T_3 = T/1000$ K, using the fitting coefficients listed in Table 6. Note that these cooling rates include the effects of ortho–para interconversion in reactive collisions. In addition, it is also necessary to account for the effect on the thermal balance of the gas of transitions from $J = 0$ to 1 and vice versa. Conversion of para-H_2 to ortho-H_2 in the $J = 0 \rightarrow 1$ transition cools the gas by $170.5\,k \simeq 2.4 \times 10^{-16}$ erg per transition, while conversion of ortho-H_2 to para-H_2 in the $J = 1 \rightarrow 0$ transition heats the gas by the same amount. In thermodynamic equilibrium, the number of transitions from $J = 0$ to 1 exactly balances the number of transitions from $J = 1$ to 0, and so there is no net effect on the gas temperature. However, if the gas is not in thermodynamic equilibrium, then there can be net heating or cooling of the gas, depending upon whether the ortho-to-para ratio is greater than or less than the equilibrium value. We account for this in our model with a rate of the form

$$\Lambda_{\mathrm{H_2,H^+},0\leftrightarrow1} = 4.76 \times 10^{-24} \left[9 \exp\left(\frac{-170.5}{T}\right) x_\mathrm{p} - x_\mathrm{o}\right], \tag{35}$$

where x_o and x_p are the fractional abundances of ortho-H_2 and para-H_2, and where we have again made use of the rotational excitation and de-excitation rates of Gerlich (1990).

We note that our treatment of H_2 cooling due to collisions with H^+ does not account for the effects of rovibrational transitions, as the calculations by Krstić (2002) are not rotationally resolved. In view of the potential importance of this process in primordial gas cooling from an initially hot, ionized state, a more comprehensive treatment would be desirable.

To treat H_2 excitation by collisions with free electrons, we use the rates given by Draine, Roberge & Dalgarno (1983), based on cross-sections from Ehrhardt et al. (1968), Crompton, Gibson & McIntosh (1969) and Linder & Schmidt (1971). Draine et al. (1983) gives formulae for the collisional de-excitation rates of pure rotational transitions with $\Delta J = 2$ and pure vibrational transitions between $v = 1$, 2 and 3 and the vibrational ground state. Using these rates, we have computed the low-density para-H_2–e^- and ortho-H_2–e^- cooling rates over a wide range of temperatures, and have fitted them with functions

$$\log \Lambda_{\mathrm{H_2},e^-} = \log\left[\exp\left(\frac{-x}{kT}\right)\right] \sum_{i=0}^{5} a_i \log(T_3)^i, \tag{36}$$

where $x = 509.85k$ for para-H_2 and $x = 845k$ for ortho-H_2. The fitting coefficients are listed in Table 7. In both cases, the fit is accurate to within 10 per cent over the temperature range $10 < T < 10\,000$ K. We note that as Draine et al. (1983) do not gives rates for rotational transitions with $\Delta J > 2$ or for rovibrational transitions, our derived H_2 cooling rates will underestimate the true rates at high temperatures. However, as collisions with protons are considerably more effective at exciting H_2 than collisions with electrons (see Section 2.3.5 below), the error that this introduces into our calculations is unlikely to be large.

2.3.5 H_2 cooling: the total cooling function

In the low-density limit, the total cooling rate per H_2 molecule (with units of erg s^{-1}) is simply given by the sum of the cooling rates due to collisions with H, H_2, He, H^+ and e^-, i.e.

$$\Lambda_{\mathrm{H_2},n\rightarrow0} = \sum_k \Lambda_{\mathrm{H_2},k} n_\mathrm{k} \tag{37}$$

where $k = \mathrm{H}, \mathrm{H_2}, \mathrm{He}, \mathrm{H^+}, \mathrm{e^-}$.

At high densities, the H_2 level populations are in LTE, and the H_2 cooling rate per molecule is independent of the chemical composition of the gas and is given by

$$\Lambda_{\mathrm{H_2,LTE}} = \sum_{i,j>i} A_{ji} E_{ji} f_j, \tag{38}$$

where A_{ij} is the radiative de-excitation rate for a transition from level j to level i, E_{ji} is the corresponding energy, and f_j is the fraction of H_2 molecules in level j, computed assuming LTE. At intermediate densities, we follow Galli & Palla (1998) and write the H_2 cooling rate as

$$\Lambda_{\mathrm{H_2}} = \frac{\Lambda_{\mathrm{H_2,LTE}}}{1 + \Lambda_{\mathrm{H_2,LTE}}/\Lambda_{\mathrm{H_2},n\rightarrow0}}. \tag{39}$$

In Fig. 1, we plot $\Lambda_{\mathrm{H_2},k}$ as a function of temperature for $k = \mathrm{H}$, $\mathrm{H_2}$, He, $\mathrm{H^+}$ and $\mathrm{e^-}$. In this plot, we assume a fixed ortho–para ratio of 3:1 (corresponding to $x_\mathrm{o} = 0.75$ and $x_\mathrm{p} = 0.25$). We also include in this plot, for the purposes of comparison, the widely used Galli & Palla (1998) cooling function.

It is immediately apparent from this plot that collisions between H and H_2 are relatively ineffective at cooling the gas at low temperatures. Given equal abundances of H and H_2, collisions with H_2 provide more cooling than collisions with H for temperatures $T < 1400$ K. Similarly, collisions with He provide more cooling than collisions with H for $T < 2000$ K, while collisions with protons or electrons are more effective over the whole of the temperature range examined here, again assuming equal abundances.

Of course, in reality, the abundances of the various collision partners will generally not be equal: in low-density primordial gas, at

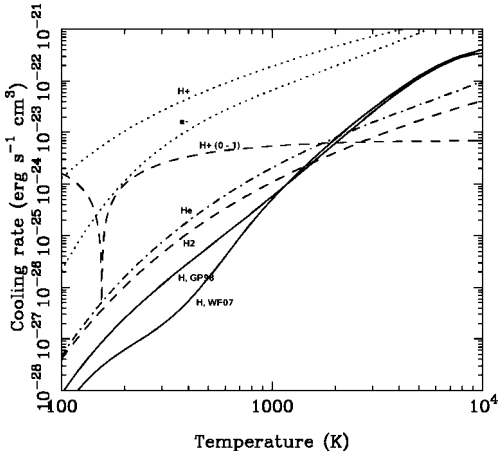

Figure 1. H_2 cooling rates per molecule, computed for $n = 10^{-4}$ cm^{-3}, for collisions with H (lower solid line), H_2 (lower dashed line), He (dash–dotted line), e^- (lower dotted line), and H^+ (upper dotted line; note that this rate excludes the effects of transitions between the ortho and para ground states). In every case an ortho–para ratio of 3:1 is assumed. Transitions between the ortho and para ground states, brought about by collisions with H^+, cool the gas at $T \gtrsim 150$ K, and heat it at lower temperatures; note, however, that the low-temperature heating is a consequence of our adoption of a temperature-independent ortho–para ratio. Also shown is the widely used Galli & Palla (1998) cooling function (upper solid line), which considers only collisions between H and H_2.

the temperature of interest here, atomic hydrogen is by far the most abundant species. Typically, in gas undergoing gravitational collapse within a small protogalaxy ($T_{\rm vir} < 10\,000$ K) forming in a region of the intergalactic medium not yet affected by stellar feedback, one finds abundances relative to atomic hydrogen of $x_{\rm He} = 0.0825$ for He, $x_{\rm H_2} \sim 10^{-3}$ for H_2 and $x_{\rm H^+} \simeq x_{\rm e^-} \sim 10^{-4}$ for protons and electrons. If these relative abundances are taken into account, then atomic hydrogen becomes comparatively more effective. Collisions with H_2 become completely unimportant for the whole of the temperature range studied, and collisions with electrons can also be neglected. However, collisions with helium remain important at low temperatures, and in fact dominate the H_2 cooling rate for $T < 650$ K, despite the significantly larger abundance of hydrogen relative to helium. Collisions with protons are also important at $T \lesssim 400$ K, in spite of the low proton abundance.

In gas cooling from an initially ionized state, similar conclusions hold regarding the relative importance of collisions with H, H_2 and He. However, in this case, values for $x_{\rm H^+}$ and $x_{\rm e^-}$ that are 10–100 times larger are not uncommon, and the effects of H_2–H^+ and H_2–e^- collisions are therefore much greater.

It is also interesting to compare the relative importance of the various processes if one adopts the Galli & Palla (1998) rate for cooling from H_2–H collisions in place of our value derived from Wrathmall & Flower (2007). Fig. 1 demonstrates that the Galli & Palla cooling rate provides significantly more cooling at $T < 1000$ K than the newer Wrathmall & Flower cooling rate, with the rates differing most significantly at temperatures $300 \lesssim T \lesssim 500$ K, where the Galli & Palla rate provides almost five times more cooling than the comparable Wrathmall & Flower rate. Because of this, collisions with He and with protons and electrons are less effective in comparison to collisions with H at $T < 1000$ K when one uses the Galli & Palla rate. Nevertheless, even though it is no longer the dominant process, cooling from H_2–He collisions remains important at low temperatures, as it can contribute 20–30 per cent of the total H_2 cooling rate. Furthermore, H_2–H^+ and H_2–e^- collisions will also still be important if the fractional ionization of the gas is large ($x_{\rm H^+} \gtrsim 10^{-3}$).

We should note at this point that we are not the first authors to highlight the potential importance of H_2–He and H_2–H^+ collisions for cooling primordial gas. Le Bourlot et al. (1999) include the effects of H_2–He collisions in their calculations of the H_2 cooling function, as do Santoro & Shull (2006); the importance of helium is also discussed at some length in Flower et al. (2000a). The possible importance of H_2–H^+ collisions was noted by Galli & Palla (1998) and their effects were examined in more detail by Flower & Pineau des Forêts (2000b) and Flower et al. (2000a), although only pure rotational transitions were considered. On the other hand, to the best of our knowledge, we are the first authors to consider the effects of H_2–e^- collisions in primordial gas.

Finally, although in this section we have given fits to the cooling rates of ortho-H_2 and para-H_2 separately, since we are interested in the effects of varying the ortho–para ratio, we recognize that for some purposes it may be useful to have the rates for a gas that has the often-assumed 3:1 mix of ortho- and para-H_2. In Table 8, we list fits to the low-density H_2 cooling rates due to collisions with H, H_2, He, H^+ and e^- for this case. All of these fits are of the form

$$\log \Lambda_{\rm H_2} = \sum_{i=0}^{5} a_i \log(T_3)^i, \tag{40}$$

where $T_3 = T/1000$ K and the accuracies are comparable to the accuracies of the separate ortho- and para-H_2 fits. Note that the H_2–H^+ rate quoted here does not include the effects of collisional transitions from $J = 0$ to 1 or vice versa. However, this can be included through the use of equation (35) with $x_{\rm p} = 0.25$ and $x_{\rm o} = 0.75$ for the 3:1 ortho–para ratio case.

2.3.6 *H_2 cooling: sensitivity to the ortho–para ratio*

In Fig. 2 we compare three different H_2 cooling rates: one for pure ortho-H_2, one for pure para-H_2, and one for which we assumed the standard 3:1 ortho–para ratio. In each case, we assume that $n \ll n_{\rm crit}$, so that we are in the low-density limit, and adopt fractional abundances relative to hydrogen of $x_{\rm He} = 0.0825$, $x_{\rm H_2} = 0.001$ and $x_{\rm H^+} = x_{\rm e^-} = 10^{-4}$ for He, H_2, H^+ and electrons, respectively. Note that at $T < 230$ K in the ortho-H_2 case and for $T < 98$ K in the 3:1 ratio case, collisional conversion of ortho-H_2 in the $J = 1$ rotational level to para-H_2 in the $J = 0$ rotational level by protons heats the gas, and that the lowest temperature portions of the curves plotted in Fig. 2 for these two cases therefore represent *heating* rates.

The figure demonstrates the importance of the ortho–para H_2 ratio in determining the H_2 cooling rate at temperatures below a few hundred K. For instance, at $T = 300$ K, there is a difference of an order of magnitude between the cooling rate of para-H_2 and the cooling rate of ortho-H_2. Because of this large disparity, para-H_2 will provide most of the contribution to the H_2 cooling rate at these temperatures even in gas that contains primarily ortho-H_2; e.g. it is the 25 per cent of para-H_2 that provides most of the cooling in the 3:1 case. Consequently, relatively small deviations in the ortho–para ratio may have a large effect on the low-temperature H_2 cooling rate.

Furthermore, although the specific values for the cooling rates plotted in Fig. 2 are sensitive to our assumed chemical abundances, the basic point that the low-temperature H_2 cooling rate is highly sensitive to the assumed ortho–para ratio is robust, as it is a consequence of the difference in the energy separations of the lowest levels of para-H_2($E_{20}/k = 509.85$ K) and ortho-H_2($E_{31}/k = 844.65$ K).

Table 8. Fitting coefficients for H_2 cooling rates, for a 3:1 ortho–para ratio.

Species	Temperature range (K)	Coefficients
H	$10 < T \leqslant 100$	$a_0 = -16.818\,342$
		$a_1 = 37.383\,713$
		$a_2 = 58.145\,166$
		$a_3 = 48.656\,103$
		$a_4 = 20.159\,831$
		$a_5 = 3.847\,9610$
H	$100 < T \leqslant 1000$	$a_0 = -24.311\,209$
		$a_1 = 3.569\,2468$
		$a_2 = -11.332\,860$
		$a_3 = -27.850\,082$
		$a_4 = -21.328\,264$
		$a_5 = -4.251\,9023$
H	$1000 < T \leqslant 6000$	$a_0 = -24.311\,209$
		$a_1 = 4.645\,0521$
		$a_2 = -3.720\,9846$
		$a_3 = 5.936\,9081$
		$a_4 = -5.510\,8047$
		$a_5 = 1.553\,8288$
H_2	$100 < T \leqslant 6000$	$a_0 = -23.962\,112$
		$a_1 = 2.094\,337\,40$
		$a_2 = -0.771\,514\,36$
		$a_3 = 0.436\,933\,53$
		$a_4 = -0.149\,132\,16$
		$a_5 = -0.033\,638\,326$
He	$10 < T \leqslant 6000$	$a_0 = -23.689\,237$
		$a_1 = 2.189\,2372$
		$a_2 = -0.815\,204\,38$
		$a_3 = 0.290\,362\,81$
		$a_4 = -0.165\,961\,84$
		$a_5 = 0.191\,913\,75$
H^+	$10 < T \leqslant 10\,000$	$a_0 = -21.716\,699$
		$a_1 = 1.386\,5783$
		$a_2 = -0.379\,152\,85$
		$a_3 = 0.114\,536\,88$
		$a_4 = -0.232\,141\,54$
		$a_5 = 0.058\,538\,864$
e^-	$10 < T \leqslant 200$	$a_0 = -34.286\,155$
		$a_1 = -48.537\,163$
		$a_2 = -77.121\,176$
		$a_3 = -51.352\,459$
		$a_4 = -15.169\,160$
		$a_5 = -0.981\,203\,22$
e^-	$200 < T \leqslant 10\,000$	$a_0 = -22.190\,316$
		$a_1 = 1.572\,8955$
		$a_2 = -0.213\,351\,00$
		$a_3 = 0.961\,497\,59$
		$a_4 = -0.910\,231\,95$
		$a_5 = 0.137\,497\,49$

2.3.7 HD cooling

To model HD cooling, we use the cooling function of Lipovka, Núñez-López & Avila-Reese (2005). This parameterization of the HD cooling rate assumes that HD–H collisions make the dominant contribution. This is a much safer assumption in the case of HD cooling than in the case of H_2 cooling. Excitation rate coefficients for HD–H collisions are typically much larger than for H_2–H collisions, and Flower et al. (2000a) show that they are comparable to the excitation rates for HD–He or HD–H_2 collisions. As $n_{\rm H} \gg n_{\rm He} \gg n_{\rm H_2}$ in the conditions of interest here, this means that the HD–H contribution will dominate.

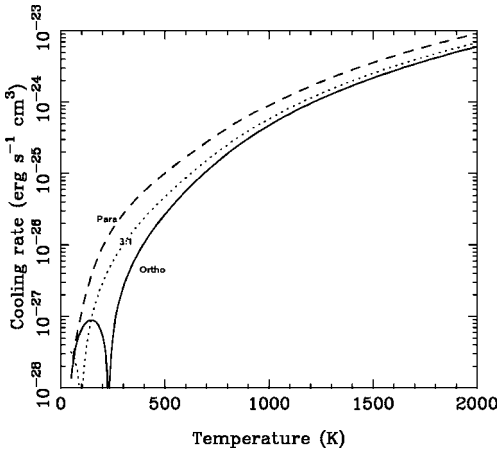

Figure 2. Comparison of the H_2 cooling rate per H_2 molecule, for gas with only ortho-H_2 (solid line), para-H_2 (dashed line) or a 3:1 mix of ortho- and para-H_2 (dotted line). We assume that $x_{\rm He} = 0.0825$, $x_{\rm H_2} = 0.001$ and $x_{\rm H^+} = x_{\rm e^-} = 10^{-4}$. Note that for $T < 230$ K in the ortho-H_2 case and $T < 98$ K in the 3:1 ratio case, the rate plotted is the net heating rate, after accounting for heating due to the collisional conversion of $J = 1$ ortho-H_2 to $J = 0$ para-H_2 by protons.

The larger excitation rates for HD–H collisions also reduce the importance of collisions with protons or electrons. Although accurate excitation rate coefficients for HD–H^+ or HD–e^- collisions do not appear to be available, it seems reasonable to assume that they will be of a similar order of magnitude to the corresponding processes with H_2. If so, then in the $T < 200$ K temperature regime in which HD cooling is important, collisions with electrons or protons become comparable to collisions with atomic hydrogen only for fractional ionizations $x \gtrsim 0.1$. To find such a large fractional ionization in gas this cold would appear to be highly unlikely, and so it seems relatively safe to neglect the effects of collisions with protons or electrons.

Although the Lipovka et al. (2005) parameterization of the HD cooling rate is formally valid only in the temperature range $100 < T < 2 \times 10^4$ K, we have compared its behaviour at lower temperatures with an explicit calculation of the cooling rate made using radiative de-excitation rates from Abgrall, Roueff & Viala (1982) and collisional rates extrapolated from those computed by Wrathmall et al. (2007). We find that the Lipovka et al. (2005) rate remains reasonably accurate down to temperatures as low as 50 K, with errors no greater than 20 per cent, and that even at $T = 30$ K it remains accurate to within a factor of 2. At temperatures $T \gg 100$ K, the Lipovka et al. (2005) cooling rate slightly underestimates the effects of HD cooling compared to the newer calculations of Wrathmall et al. (2007), presumably owing to the more accurate vibrational excitation rates used in the latter, but the differences are relatively small and in any case occur in the temperature regime in which H_2 cooling dominates. The breakdown of the Lipovka et al. (2005) fit at very high temperatures ($T > 20\,000$ K) is unimportant, as the gas in our models never exceeds this temperature, nor could HD cooling ever be significant in this temperature regime where the cooling from the Lyman α line of neutral hydrogen peaks.

To correctly model the effects of HD cooling at low temperatures, it is necessary to take the effects of the CMB into account. We do this approximately, by using a modified HD cooling rate, $\Lambda'_{\rm HD}$, defined

as

$$\Lambda'_{\rm HD} = \Lambda_{\rm HD}(T) - \Lambda_{\rm HD}(T_{\rm CMB}), \quad (41)$$

where $\Lambda_{\rm HD}(T)$ and $\Lambda_{\rm HD}(T_{\rm CMB})$ are the unmodified HD cooling rates at the gas temperature T and the CMB temperature $T_{\rm CMB}$, respectively.

The quoted range of densities for which the Lipovka et al. (2005) cooling function is valid is $1 < n < 10^8\,{\rm cm}^{-3}$. To extend the range of the cooling function to densities $n < 1\,{\rm cm}^{-3}$, we assume that at these densities the cooling rate per molecule is directly proportional to n, and hence that

$$\Lambda_{\rm HD}(n = n') = n' \Lambda_{\rm HD}(n = 1) \quad (42)$$

for $n' \leqslant 1\,{\rm cm}^{-3}$, where $\Lambda_{\rm HD}(n)$ is the cooling rate per HD molecule (with units erg s^{-1}) at gas number density n. To extend the cooling function to high densities, $n > 10^8\,{\rm cm}^{-3}$, we assume that the HD molecule is in LTE and thus has a cooling rate per molecule that is independent of density. In this regime,

$$\Lambda_{\rm HD}(n > 10^8) = \Lambda_{\rm HD}(n = 10^8). \quad (43)$$

In view of the fact that $1 \ll n_{\rm cr,HD} \ll 10^8\,{\rm cm}^{-3}$, where $n_{\rm cr,HD}$ is the HD critical density, both of these assumptions appear well justified.

2.3.8 H_2^+, HD^+ and D_2^+ cooling

In view of its possible importance in hot, ionized gas (see Yoshida et al. 2007), we include the effects of vibrational cooling from the H_2^+ molecular ion, as well as from its deuterated analogues HD^+ and D_2^+.

At low densities, the main contributions to the H_2^+ cooling rate come from excitations by collisions with electrons and with neutral hydrogen (Suchkov & Shchekinov 1978). We have computed the cooling rate due to collisions with electrons, using the vibrational rates of Sarpal & Tennyson (1993) for excitations from $v = 0$ to 1 and 2; excitations to higher vibrational states ($v = 3$–8) are also included, under the assumption that the de-excitation rates for these transitions are comparable to the de-excitation rate from $v = 2$ to 0. We note that even at temperatures as high as 10^4 K, at least half of the total cooling comes from excitations to $v = 1$ and 2, and so our approximate treatment of transitions to the higher vibrational states makes the cooling rate uncertain by at most a factor of a few at high temperatures (and by far less than this at low temperatures). The resulting H_2^+ cooling rate, $\Lambda_{\rm e,H_2^+}$, is given at $T \leqslant 2000$ K by

$$\Lambda_{\rm e,H_2^+} = 1.1 \times 10^{-19} T^{-0.34} \exp\left(-\frac{3025}{T}\right), \quad (44)$$

and at $T > 2000$ K by

$$\Lambda_{\rm e,H_2^+} = 3.35 \times 10^{-21} T^{0.12} \exp\left(-\frac{3025}{T}\right). \quad (45)$$

For H_2^+ cooling arising from collisions with H, we use at $T \leqslant 1000$ K a rate

$$\Lambda_{\rm H,H_2^+} = 1.36 \times 10^{-22} \exp\left(-\frac{3152}{T}\right), \quad (46)$$

and at $T > 1000$ K a rate

$$\Lambda_{\rm H,H_2^+} = {\rm dex}[-36.42 + 5.95 \log(T) - 0.526 \log(T)^2]. \quad (47)$$

The high-temperature rate is a fit made by Galli & Palla (1998) to the rate given in Suchkov & Shchekinov (1978); note that owing to a normalization error, the rates given for $\Lambda_{\rm H,H_2^+}$ and $\Lambda_{\rm e,H_2^+}$ in fig. A2 of Galli & Palla (1998) are too large by a factor of 10. The low-temperature rate given here is a physically reasonable extrapolation of the Suchkov & Shchekinov (1978) rate that has the correct exponential fall-off at low temperature.

At high densities, the vibrational levels of H_2^+ will be in LTE. In this regime, the cooling rate per H_2^+ ion is given approximately by

$$\Lambda_{\rm LTE,H_2^+} = 2.0 \times 10^{-19} T^{0.1} \exp\left(-\frac{3125}{T}\right). \quad (48)$$

To compute this rate, we included contributions from all vibrational states $v \leqslant 8$ and used level energies from Karr & Hilico (2006) and radiative transition rates from Posen, Dalgarno & Peek (1983). The effects of rotational excitation were not included, but are unlikely to change this expression by a large amount, owing to the very small transition rates associated with these transitions.

At intermediate densities, we assume that the H_2^+ vibrational cooling rate per H_2^+ ion is given approximately by the function

$$\Lambda_{\rm H_2^+} = \frac{\Lambda_{\rm LTE,H_2^+}}{1 + \Lambda_{\rm LTE,H_2^+} / \Lambda_{n \rightarrow 0,\rm H_2^+}}, \quad (49)$$

where $\Lambda_{n \rightarrow 0,\rm H_2^+}$ is the cooling rate per H_2^+ ion in the low-density limit, and is given by

$$\Lambda_{n \rightarrow 0,\rm H_2^+} = \Lambda_{\rm e,H_2^+} n_{\rm e^-} + \Lambda_{\rm H,H_2^+} n_{\rm H}. \quad (50)$$

To model cooling from vibrational transitions in HD^+, we assume, in the absence of better information, that the low-density cooling rate is the same as that used for H_2^+. However, since HD^+ has much larger radiative transition rates than H_2^+, the LTE cooling rate for HD^+ is much larger than that for H_2^+. We have calculated the HD^+ LTE cooling rate per ion using level energies from Karr & Hilico (2006) and transition rates from Peek, Hashemi-Attar & Beckel (1979), and have fitted it with the function

$$\Lambda_{\rm LTE,HD^+} = 1.09 \times 10^{-11} T^{0.03} \exp\left(-\frac{2750}{T}\right) \quad (51)$$

at temperatures $T \leqslant 1000$ K and

$$\Lambda_{\rm LTE,HD^+} = 5.07 \times 10^{-12} T^{0.14} \exp\left(-\frac{2750}{T}\right) \quad (52)$$

at $T > 1000$ K. For densities between the low-density and LTE limits, we use a function of the form of equation (49) to compute the HD^+ cooling rate.

Finally, to model D_2^+ cooling, we simply assume that the same rates apply as for H_2^+ cooling. In practice, the very small size of the typical D_2^+ abundance renders this process irrelevant.

2.3.9 Other processes

In addition to the coolants listed above, we also include radiative cooling from the electronic excitation of H, He and He^+ using rates taken from Cen (1992) and Bray et al. (2000), Compton cooling (again using a rate from Cen 1992) and bremsstrahlung (using the rates given in Shapiro & Kang 1987).

Moreover, we also include the effects of chemical cooling from the collisional ionization of H, He and He^+ (reactions 12, 17 and 18), collisional dissociation of H_2 (reactions 8–11), the destruction of H_2 by charge transfer (reaction 7), and the recombination of H^+, He^+ and He^{++} (reactions 13, 19 and 20), as well as chemical heating arising from the formation of H_2 via reactions (2) and (4).

Further details of our treatment of these processes can be found in Glover & Jappsen (2007).

2.4 Model set-up and initial conditions

We model the chemical and thermal evolution of primordial gas within the context of two simple toy models for its dynamical evolution. In one, we assume that the gas evolution is isobaric. In this model, the gas temperature evolves as

$$\frac{\mathrm{d}T}{\mathrm{d}t} = -\frac{\gamma-1}{\gamma}\frac{\mu}{k}\frac{\Lambda-\Gamma}{\rho} + T\frac{\mathrm{d}\ln\mu}{\mathrm{d}t} + \frac{T}{\gamma-1}\frac{\mathrm{d}\ln\gamma}{\mathrm{d}t}, \quad (53)$$

where μ is the mean molecular weight of the gas (in grams), Λ and Γ are the total cooling and heating rates per unit volume, and the other symbols have their usual meanings. The rate of change of μ can be easily determined from the chemical rate equations. For the adiabatic index γ, we use the expression

$$\gamma = \frac{5 + 5x_{\rm He} + 5x_{\rm e} - 3x_{\rm H_2}}{3 + 3x_{\rm He} + 3x_{\rm e} - x_{\rm H_2}}, \quad (54)$$

where $x_{\rm He}$, $x_{\rm H_2}$ and $x_{\rm e}$ are the fractional abundances of helium, H_2 and free electrons relative to the abundance of hydrogen nuclei. In practice, $x_{\rm H_2}$ remains small at all densities encountered in our isobaric models, and so $\gamma \simeq 5/3$ throughout. Finally, at any point in the evolution of the gas, we can relate the gas density to the temperature by

$$\rho = \left(\frac{T_{\rm i}}{T}\right)\left(\frac{\mu}{\mu_{\rm i}}\right)\rho_{\rm i}, \quad (55)$$

where $\rho_{\rm i}, T_{\rm i}$ and $\mu_{\rm i}$ are the initial values of the density, temperature and mean molecular weight, respectively.

In the other model, we assume that the gas undergoes gravitational collapse at the free-fall rate. In this model, the gas temperature evolves as

$$\frac{\mathrm{d}T}{\mathrm{d}t} = \frac{\gamma-1}{\rho}\left[T\frac{\mathrm{d}\rho}{\mathrm{d}t} - \frac{\mu}{k}(\Lambda-\Gamma)\right] + \frac{T}{\gamma-1}\frac{\mathrm{d}\gamma}{\mathrm{d}t} + T\frac{\mathrm{d}\ln\mu}{\mathrm{d}t}, \quad (56)$$

and the gas density evolves as

$$\frac{\mathrm{d}\rho}{\mathrm{d}t} = \frac{\rho}{t_{\rm ff}}, \quad (57)$$

where $t_{\rm ff} = \sqrt{3\pi/32G\rho}$ is the free-fall time.

The first of these models approximates the case of gas that has been strongly shocked (e.g. by a supernova blast wave or in a halo merger) but that is not yet gravitationally unstable. The free-fall collapse model approximates the other extreme case, in which gas is highly gravitationally unstable, and contracts at the maximal rate. Realistically, the dynamical evolution of gas involved in high-redshift structure formation probably lies somewhere in between these two cases.

Although one could use far more sophisticated models for the dynamical evolution of the gas (see e.g. Yoshida et al. 2007), our use of these simple models allows us to rapidly explore the effects of the various different sources of uncertainty discussed in this paper, and to highlight which are deserving of more numerically expensive three-dimensional studies, and which are unimportant and can be safely ignored in future work.

To evolve the coupled set of chemical rate equations and the thermal energy equation we use the DVODE solver of Brown, Byrne & Hindmarsh (1989).

We adopt standard helium and deuterium abundances of $x_{\rm He} = 0.0825$ and $x_{\rm D} = 2.6 \times 10^{-5}$ relative to hydrogen (Molaro 2007), and begin our simulations with gas in which hydrogen and deuterium are fully ionized and the helium is singly ionized. The initial abundances of all other species are set to zero.

We fix the initial temperature at $T_{\rm i} = 20\,000$ K, and examine models with three different initial densities: $n_{\rm i} = 0.03$, 1 and 30 cm^{-3}. We run all of our models for two different redshifts, $z = 10$ and 20; the latter value is perhaps more appropriate for the study of the earliest generations of star formation, but the former allows us to look at the effects of having a CMB temperature that is much smaller than the temperature that the gas can reach through H_2 cooling alone.

3 RESULTS

3.1 Ortho–para ratio

In order to establish the effect that variations in the H_2 ortho–para ratio have on the thermal evolution of primordial gas, we considered four separate cases: the two limiting cases in which all of the H_2 is in the form of ortho- or para-hydrogen, respectively, a third case in which the standard ratio of 3:1 was assumed, and a final case in which the ortho–para ratio was determined self-consistently, although approximately, from the populations of the lowest four rotational levels, as outlined in Section 2.2.

In Fig. 3(a), we show how the gas temperature evolves as a function of density for these four cases in two free-fall collapse models with initial density $n_{\rm i} = 0.03$ cm^{-3} for redshifts $z = 10$ (lower set of curves) and $z = 20$ (upper set of curves). Figs 3(b) and (c) show similar results for models with initial densities $n_{\rm i} = 1$ and 30 cm^{-3}, respectively. In each figure, the dashed and dash–dotted curves correspond to calculations in which the H_2 is all in ortho or para form, respectively, the solid curves correspond to the calculations that assume an ortho–para ratio of 3:1 and the dotted curves correspond to the calculations in which the ortho–para ratio was determined dynamically. The horizontal dashed lines give the CMB temperature at $z = 20$ (upper line) and $z = 10$ (lower line).

Fig. 3 demonstrates that there are significant differences between the temperature evolution in the pure ortho-H_2, pure para-H_2 and 3:1 ratio calculations. The para-H_2 and 3:1 ratio calculations differ primarily at $n < 10^5$ cm^{-3}, with temperatures differing by as much as 50 per cent at $n \sim 100$ cm^{-3}. At $n > 10^5$ cm^{-3}, however, the simulations become convergent, and little difference remains in the temperature evolution. The ortho-H_2 simulations show an even greater difference in behaviour. In most of these simulations, the gas temperature remains significantly larger than in the para-H_2 or 3:1 ratio runs, differing by a factor of 2 or more, and failing to converge with the other simulations even at $n > 10^5$ cm^{-3}. The gas temperature in most of the ortho-H_2 simulations remains above 100 K throughout the collapse, and although a comparison of cooling rates shows that HD cooling does become dominant in these simulations, it does not succeed in driving down the temperature to the same extent as in the other runs. The one exception is the simulation with $n_{\rm I} = 0.03$ cm^{-3} and $z = 10$, which does cool significantly below 100 K and which converges with the corresponding para-H_2 and 3:1 ratio calculations.

Despite the apparent sensitivity of the temperature evolution to the ortho–para ratio, Fig. 3 demonstrates that there is essentially no difference between the results of calculations in which the ortho–para ratio is fixed at 3:1 or calculated self-consistently from the H_2 level populations. Fig. 4 helps to demonstrate why this is so. In the figure, we show the dependence of the ortho–para ratio on the gas temperature in a representative free-fall collapse model with $z = 20$ and $n_{\rm i} = 1$ cm^{-3}. At temperatures $T > 200$ K, the ortho–para ratio is approximately three, both at low densities (solid line, lower branch) and at high densities (solid line, upper branch). At lower temperatures, the ortho–para ratio falls off steeply with decreasing

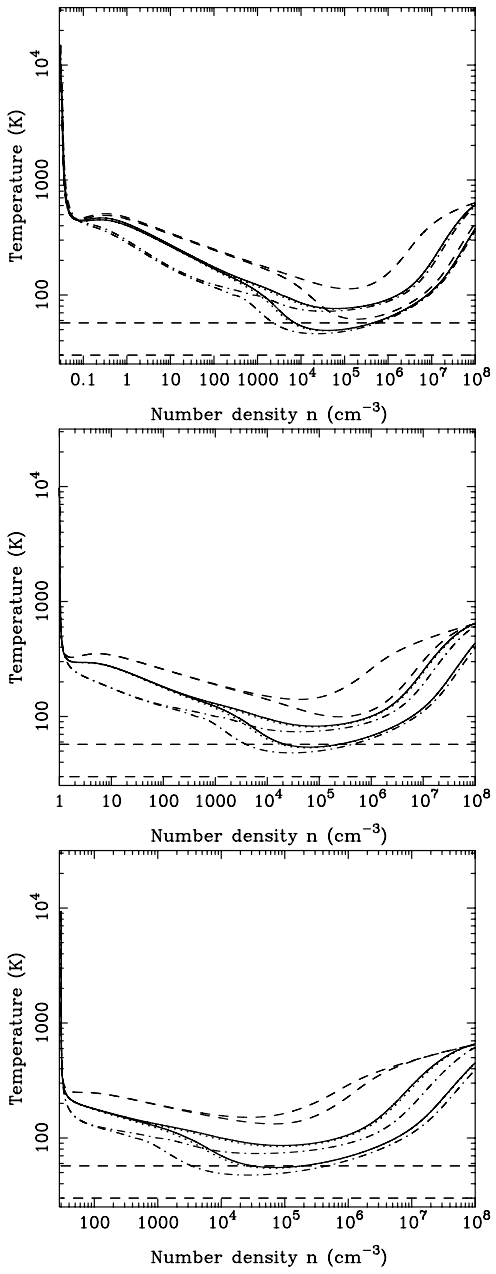

Figure 3. (a) Temperature evolution as a function of gas number density in free-fall collapse models with initial density $n_i = 0.03\,\mathrm{cm}^{-3}$ and initial redshifts $z = 20$ (upper set of curves) and $z = 10$ (lower set of curves). Four cases are examined: gas with pure ortho-H_2 (dashed curves), pure para-H_2 (dash–dotted curves), a 3:1 ortho–para ratio (solid curves) and an ortho–para ratio determined by solution of the simplified level population calculation discussed in Section 2.2 (dotted curves; note that these are barely distinguishable from the solid lines in the plot). The CMB temperature at $z = 10$ and 20 is indicated by the horizontal dashed lines. (b) As (a), but for gas with $n_i = 1\,\mathrm{cm}^{-3}$. (c) As (a), but for gas with $n_i = 30\,\mathrm{cm}^{-3}$.

temperature, and at the lowest temperature reached by the gas, $T \simeq 81$ K, para-hydrogen is almost as abundant as ortho-hydrogen. However, in this calculation, HD cooling dominates over H_2 cooling at a temperature $T = 135$ K (indicated in the figure by the vertical solid line). At this temperature the ortho–para ratio is ∼2.4, and so the H_2 cooling rate does not differ greatly from the rate that we obtain by assuming a fixed ortho–para ratio of 3:1. In other words, at

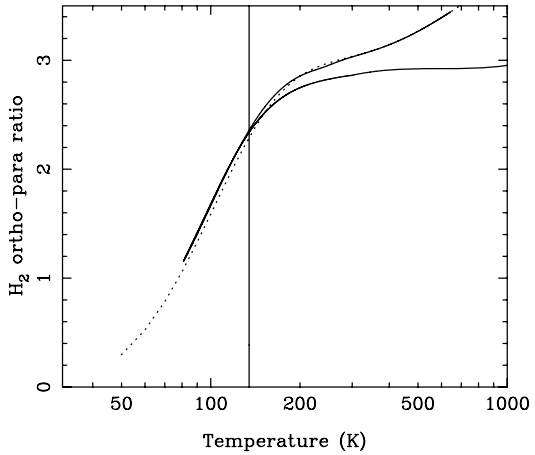

Figure 4. Ortho–para ratio as a function of gas temperature in a free-fall collapse model with $z = 20$ and $n_i = 1\,\mathrm{cm}^{-3}$. The collapsing gas evolves initially towards lower temperatures along the lower branch of the solid line, before progressing back toward higher temperatures along the upper branch as the gas heats up at high density. The dotted line gives the equilibrium ortho–para ratio for our simplified model H_2 molecule. The vertical solid line indicates the temperature below which HD cooling becomes dominant.

the temperatures where the true H_2 cooling rate differs significantly from the H_2 cooling rate in the 3:1 ortho–para case, H_2 cooling is itself unimportant, and HD cooling dominates. We have verified that the same explanation also serves to explain the results of our other free-fall collapse models.

Finally, to check that our conclusions do not depend on our choice of dynamical model, we have examined the behaviour of isobarically evolving gas in the same four cases, as illustrated in Fig. 5. We see that again the temperature evolution is sensitive to extreme variations of the ortho–para ratio, but that the results of the self-consistent calculation are barely distinguishable from those of the calculation assuming a 3:1 ortho–para ratio. Further investigation demonstrates that the reason for this similarity is the same as in the free-fall collapse case: at temperatures where H_2 cooling is significant, the ortho–para ratio remains close to three, while at the low temperatures at which it differs significantly from three, H_2 cooling is unimportant and HD cooling dominates.

We can therefore conclude that the adoption of a fixed ortho–para ratio of 3:1, although strictly speaking unjustified at $T < 200$ K, is nevertheless an adequate assumption for modelling the temperature evolution of primordial gas, and that therefore this potential source of uncertainty ultimately proves to be unimportant.

3.2 Choice of H_2 cooling function

To explore the sensitivity of the thermal evolution of primordial gas, and in particular of the ability of the gas to cool to temperatures at which HD cooling dominates, to uncertainties and omissions in the treatment of H_2 cooling, we ran a number of free-fall collapse and isobaric evolution models using different H_2 cooling functions. Our reference model (hereafter CF1) uses the cooling function outlined in Section 2.3 and used elsewhere in this paper; it includes the effects of collisions with H, H_2, He, H^+ and e^-, and an ortho–para ratio that was computed self-consistently with the evolution of the gas. We also examined the effects of omitting the H^+ and e^- contributions (CF2), and of omitting H^+, e^- and He (CF3); note that in the latter case, the H_2 cooling function essentially consists only of the H_2–H contribution, as the H_2 fractions in our calculations are too small for

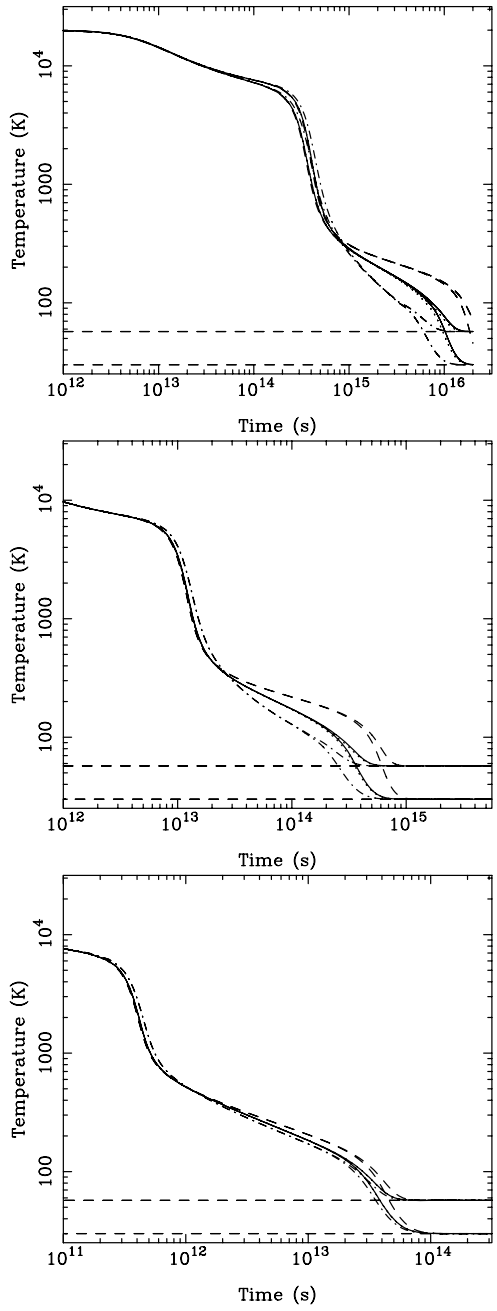

Figure 5. (a) Temperature evolution as a function of time in a set of models in which the gas evolution is isobaric. These models have an initial gas number density $n_i = 0.03\,\mathrm{cm}^{-3}$, and results are plotted for both $z = 10$ (lower set of lines) and $z = 20$ (upper set of lines). Four cases are examined: gas with pure ortho-H_2 (dashed lines), pure para-H_2 (dash–dotted lines), a 3:1 ortho–para ratio (solid lines) and an ortho–para ratio determined from the level populations of our model H_2 molecule (dotted lines; note that again these are barely distinguishable from the solid lines in the plot). The CMB temperature at $z = 10$ and 20 is indicated by the horizontal dashed lines. (b) As (a), but for an initial number density $n_i = 1\,\mathrm{cm}^{-3}$. (c) As (a), but for an initial number density $n_i = 30\,\mathrm{cm}^{-3}$.

H_2–H_2 collisions to ever become important. Finally, we examine the effect of including only the H_2–H contribution, but using the Galli & Palla (1998) cooling rate instead of the Wrathmall & Flower (2007) rate (CF4). Note that case CF4 assumes a fixed ortho–para ratio of 3:1, while the other treatments determine the ortho–para ratio self-consistently, as outlined above. However, the results of the previous section demonstrate that in practice this should not be a major source of error.

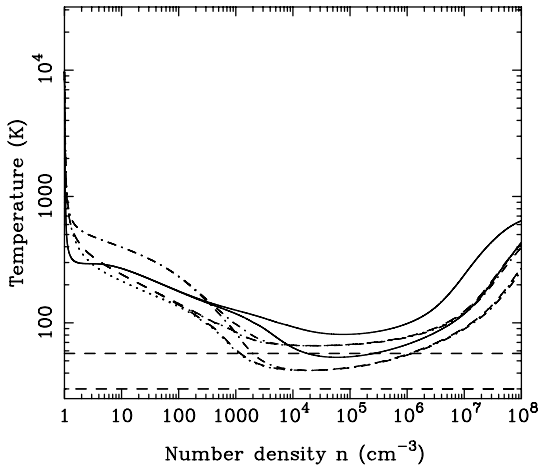

Figure 6. Temperature evolution as a function of gas number density in free-fall collapse models with initial density $n_i = 1\,\mathrm{cm}^{-3}$ and initial redshifts $z = 10$ (upper curves) and $z = 20$ (lower curves). The horizontal dashed lines indicate the CMB temperature at these redshifts. Four different treatments of H_2 cooling are compared: our full model, CF1 (solid line); two variants of this model, one which omits H^+ and e^- collisions (CF2; dashed line), and one which omits H^+, e^- and He collisions (CF3; dot–dashed line); and the treatment used in most previous studies, which includes only collisions with H, but uses the Galli & Palla (1998) cooling rate rather than the Wrathmall & Flower (2007) rate.

In Fig. 6, we show the temperature evolution of the gas as a function of density in two free-fall collapse models with an initial density $n_i = 1\,\mathrm{cm}^{-3}$ and redshifts $z = 10$ and 20. The solid, dashed, dot–dashed and dotted lines correspond to CF1, CF2, CF3 and CF4, respectively. There are two important points to note about this plot.

First, it is clear that the temperature evolution of the gas in case CF1 differs from that in the other models over the whole range of density studied here. Although the initial cooling of the gas is rapid in this model, this only lasts until the temperature reaches $T \sim 300\,\mathrm{K}$. At lower temperatures, the cooling of the gas slows down dramatically, allowing cooling in the other models to catch up and surpass it. The gas reaches a minimum temperature of 81 K in the $z = 20$ run and 53 K in the $z = 10$ run, significantly higher than the limits set by the CMB.

Secondly, the temperature evolution of the gas in models CF2, CF3 and CF4 differs noticeably at densities $n < 10^4\,\mathrm{cm}^{-3}$ and temperatures $T < 500\,\mathrm{K}$. The behaviour of models CF2 and CF4 is surprisingly similar, given the difference in physical content of these two models, but the behaviour of model CF3 is clearly different, with the gas in the latter model cooling less rapidly than in the other two. At densities higher than $10^4\,\mathrm{cm}^{-3}$, however, all three models converge, and by the end of the simulation, the temperatures differ by no more than 10 per cent. We obtain very similar results for free-fall collapse models with $n_i = 0.03\,\mathrm{cm}^{-3}$ and $n_i = 30\,\mathrm{cm}^{-3}$.

The rapid cooling of the gas at early times in case CF1 is an obvious consequence of our inclusion of the cooling arising from H_2–H^+ and H_2–e^- collisions, but the relatively slow rate of cooling at later times (compared to the other models) at first seems somewhat counterintuitive: by adding extra coolants, we have made the gas cool more slowly! However, this puzzle is easy to solve if we examine the evolution of the H_2 fraction in these simulations. In

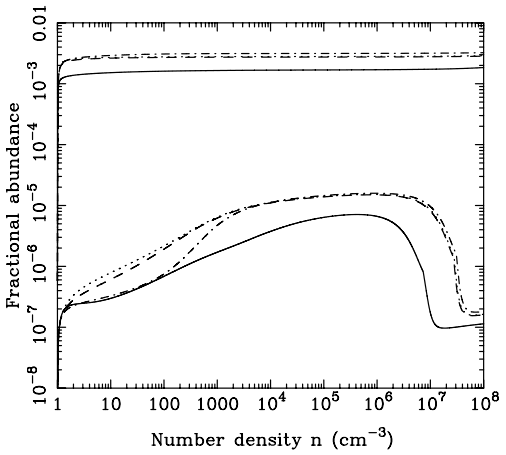

Figure 7. Evolution of H_2 and HD abundances as a function of gas number density in free-fall collapse models with initial density $n_i = 1\,cm^{-3}$ and initial redshift $z = 20$. We compare the behaviour for four different treatments of the H_2 cooling: CF1 (solid line), CF2 (dashed line), CF3 (dash–dotted line) and CF4 (dotted line). Full details of these treatments are given in the text.

Fig. 7 we show how the H_2 and HD abundances evolve for models CF1–CF4; for clarity, we plot only the $z = 20$ case, although the behaviour in the $z = 10$ case is very similar.

Fig. 7 shows that significantly less H_2 is produced in case CF1 than in the other cases, with the difference amounting to more than a factor of 2 at late times. This is a direct result of the rapid cooling of the gas at early times in run CF1. Most of the H_2 that forms in all of the runs does so at early times, while the fractional ionization of the gas is still large. Enhanced cooling during this period reduces the rate of H^- formation (owing to the positive temperature dependence of the reaction coefficient for the formation of H^- by radiative association, reaction 1), and also increases the destruction rate of H^- by mutual neutralization (since the rate increases for decreasing T, regardless of which particular rate coefficient we adopt). The net result is a reduction in the H_2 formation rate during this critical early period, and hence a reduction in the H_2 abundance at late times.

Fig. 7 also demonstrates that this reduction in the H_2 abundance leads to a corresponding reduction in the HD abundance, which is a simple consequence of the fact that in most circumstances, reactions (39) and (41) dominate the production and destruction of HD, and are in equilibrium, implying that $x_{HD} \propto x_{H_2}$.

The differences between runs CF2, CF3 and CF4 are also easy to understand. At low densities and low temperatures, the Galli & Palla (1998) cooling function provides significantly more cooling per H_2 molecule than the Wrathmall & Flower (2007), as Fig. 2 demonstrates, and so gas in run CF4 can more easily reach a low temperature than gas in run CF3. Below a temperature of about 150 K, however, HD cooling begins to dominate in both models. As the H_2 abundance does not differ greatly between the two models, HD cooling is comparably effective in each, and the thermal evolution of the gas becomes insensitive to the choice of H_2 cooling function. The temperature curves therefore begin to converge, with this convergence becoming complete by the time that the gas reaches a density $n \simeq 10^4\,cm^{-3}$. At very high densities ($n > 10^7\,cm^{-3}$), the gas once again becomes too warm for HD cooling to dominate, as the enhancement of the HD abundance by chemical fractionation becomes much less pronounced. However, at these densities, H_2 is in LTE, and the only uncertainty in the H_2 cooling rate comes from the small uncertainties in the energies of the various rotational and vibrational levels, and in the radiative transition rates.

Including helium, as in run CF2, increases the H_2 cooling rate, particularly at low temperatures, and so the gas cools faster. However, the combination of the Wrathmall & Flower (2007) rate for H_2–H cooling with the H_2–He cooling rate presented in Section 2.3.3, scaled by the appropriate He:H ratio, coincidentally results in a total cooling rate that is similar to the Galli & Palla (1998) cooling rate: the two differ by no more than 25 per cent in the temperature range $210 < T < 1000\,K$ (assuming an ortho–para ratio of 3:1), despite the large disparity in the H_2–H cooling rates of Galli & Palla (1998) and Wrathmall & Flower (2007) at these temperatures.

The isobaric evolution models tell a similar story. Fig. 8(a) shows how the gas temperature evolves with time in two representative models with initial density $n_i = 1\,cm^{-3}$ and redshifts $z = 10$ (lower curves) and $z = 20$ (upper curves). We again find that the choice of H_2 cooling function affects the temperature evolution. Models CF2

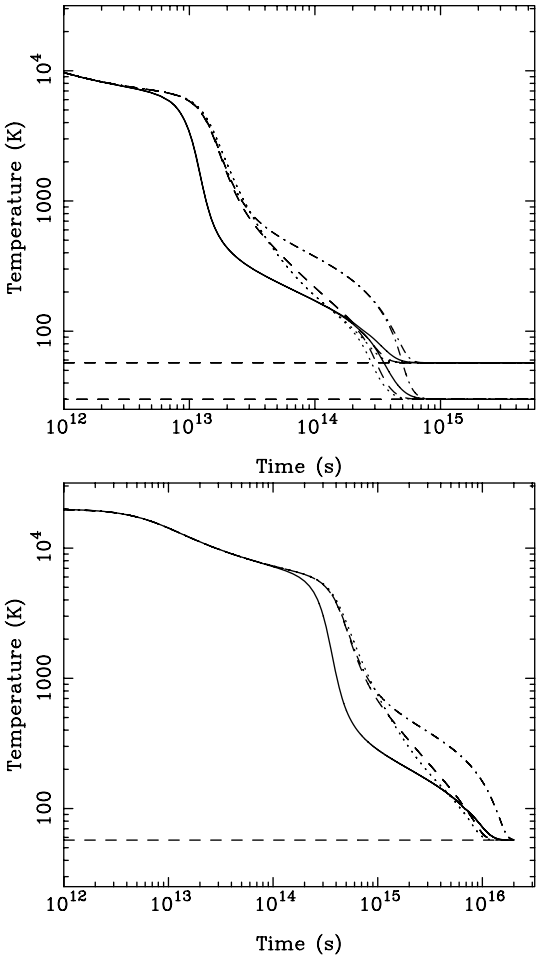

Figure 8. (a) As Fig. 6, but showing the temperature evolution versus time for a set of models in which the evolution of the gas is isobaric. The initial density was $n_i = 1\,cm^{-3}$, and results are plotted for both $z = 10$ (lower set of lines) and $z = 20$ (upper set of lines). Four different treatments of H_2 cooling are compared: CF1 (solid line), CF2 (dashed line), CF3 (dash–dotted line) and CF4 (dotted line). The horizontal dashed lines indicate the CMB temperature at redshifts $z = 10$ and 20. For reference, the Hubble time at $z = 10$ is $t_H \simeq 2.3 \times 10^{16}$ s and at $z = 20$ is $t_H \simeq 9.0 \times 10^{15}$ s, where we have adopted the standard *WMAP*3 cosmological parameters (Spergel et al. 2007). (b) As (a), but for isobaric models with $n_i = 0.03\,cm^{-3}$; note that only the $z = 20$ case is plotted.

and CF4 again barely differ, while model CF3 differs from them significantly only at low temperatures ($T < 700$ K). At high temperatures ($T \gg 700$ K), cooling in all three of these models is dominated the vibrational excitation of H_2 by hydrogen atoms, and the vibrational rates differ little between the Galli & Palla (1998) and Wrathmall & Flower (2007) treatments. On the other hand, if we include the effects of H^+ and e^- collisional excitation of H_2, as in model CF1, we see a more substantial difference in the temperature evolution of the gas, at all temperatures $T < 7000$ K. Because of the high initial ionization, H_2–H^+ collisions dominate, and the gas cools much faster than in the other models. We find similar results in our $n_i = 0.03$ and $30\,cm^{-3}$ models.

The importance of the difference in cooling time is unclear, but likely depends upon the other relevant time-scales in the problem. For instance, in the present example, the time required for the gas to cool to T_{CMB} is much less than the Hubble time t_H regardless of which treatment of H_2 cooling is used. On the other hand, in our $n_i = 0.03\,cm^{-3}$, $z = 20$ model, illustrated in Fig. 8(b), we find that $t_{cool} \simeq t_H$ for CF1, CF2 and CF4, but is approximately twice as long as the Hubble time if we use treatment CF3.

We close this section by noting that despite the differences in the temperature evolution brought about by a change in H_2 cooling function, in every case we have examined the gas remains able to cool below the temperature reachable by H_2 cooling alone. In other words, HD cooling is important in every case considered here, and the gas always reaches the regime in which HD cooling dominates. However, in the free-fall models, the minimum temperature reached by the gas is always higher than the temperature floor set by the CMB, and varies depending on whether or not we include the effects of H_2–H^+ and and H_2–e^- collisions when computing the H_2 cooling rate. If, as has been hypothesized by some authors (see e.g. Johnson & Bromm 2006), gravitational fragmentation of the gas occurs only once the gas reaches its minimum temperature, then simulations that do not include these processes will produce fragments that are too small by roughly a factor of 2. On the other hand, if the outcome of the fragmentation process is determined in part by the gas dynamics at earlier times, then the inclusion of these processes could conceivably enhance fragmentation, owing to the reduction in the cooling time of the gas at early times, and the much flatter temperature dependence of the H_2–H^+ cooling rate compared to the H_2–H cooling rate. Our very simple dynamical models do not allow us to explore these issues in any greater detail, but will hopefully motivate further work on the subject.

3.3 Uncertainties in the reaction rate coefficients

In Section 2.1, we discussed the large uncertainties that exist in some of the rate coefficients for reactions included in our chemical model. The most uncertain rates in our model are the destruction of H^- by associative detachment with H (reaction 2; see Section 2.1.1), the destruction of H^- by mutual neutralization with H^+ (reaction 5; again see Section 2.1.1), the destruction of H_2 by charge transfer with H^+ (reaction 7; see Section 2.1.2), and the three-body formation of H_2 (reactions 30 and 31; see Section 2.1.5). In the following sections, we examine the individual effects of each of these uncertainties, before concluding by placing limits on the combined effect of all four uncertainties.

Although we have examined the effects of these uncertainties for all of the combinations of n_i and z considered previously in this paper, for simplicity (and for clarity in the figures) we restrict our discussion here to one particular case: $n_i = 1\,cm^{-3}$ and $z = 20$. Unless otherwise noted, we find very similar results for all of the other combinations of redshift and density that we have studied.

3.3.1 Associative detachment and mutual neutralization

In gas cooling and recombining from an initially ionized state, the amount of H_2 formed is sensitive to the ratio between the destruction rate of H^- by associative detachment with H (reaction 2) and by mutual neutralization with H^+ (reaction 5). An increase in k_2 or a decrease in k_5 leads to associative detachment becoming the dominant destruction process at earlier times, when the fractional ionization of the gas is larger, and hence leads to a larger final H_2 fraction; conversely, a decrease in k_2 or an increase in k_5 means that mutual neutralization dominates for a longer period, and hence the final H_2 fraction is smaller. As Glover et al. (2006) have already shown, in the absence of a substantial ultraviolet background, the effect on the final H_2 fraction is not as large as might be feared: an order of magnitude change in k_2 or k_5 alters the final H_2 fraction by no more than a factor of a few. Nevertheless, this is enough to alter the temperature evolution of the gas by an appreciable amount, as we can see from Figs 9 and 10.

Fig. 9(a) shows the effect on a representative free-fall collapse model of varying the associative detachment rate while keeping the mutual neutralization rate fixed. We plot results from a model using our default value for k_2, taken from Schmeltekopf et al. (1967), and from models using 'maximal' and 'minimal' values for k_2 taken from Glover et al. (2006). The uncertainty in k_2 introduces an uncertainty into the temperature evolution that persists throughout the simulation. Gas in simulations with a high value for k_2 (and hence higher H_2 fractions) has a systematically lower temperature than the gas in simulations with a low value for k_2. The difference between the simulations is particularly pronounced for densities in the range $10^6 < n < 10^7\,cm^{-3}$. The relatively rapid increase in the gas temperature at these densities occurs because HD reaches LTE, and hence can no longer cool the gas so effectively. The causes the gas to begin heating up, which in turn reduces the HD abundance (as fractionation becomes less effective), causing the gas to warm further. The rate at which this process occurs depends upon the initial HD abundance, and hence on the H_2 abundance; reheating occurs more slowly when the H_2 abundance is large. The gas temperature in this density regime can therefore differ by a factor of 2 or more, depending on which value is chosen for k_2.

In Fig. 9(b), we show how the same variation in k_2 affects the temperature evolution in a representative isobaric model. In this case, the reduction in the H_2 fraction resulting from a decrease in k_2 systematically delays cooling relative to our reference calculation. Similarly, an increase in k_2 accelerates cooling. In the present context, what is perhaps most interesting is the time taken to reach the temperature floor set by the CMB. This occurs after $t \simeq 4 \times 10^{14}$ s in the model with the largest value of k_2 and after $t \simeq 6 \times 10^{14}$ s in the model with the smallest value of k_2. We find a similar degree of uncertainty in the cooling times in our other isobaric models.

In Fig. 10, we examine the effect of varying the mutual neutralization rate while keeping the associative detachment rate fixed. We plot results from models performed using mutual neutralization rates from Croft et al. (1999) – our default – as well as from Moseley et al. (1970) and Dalgarno & Lepp (1987). Fig. 10 shows that varying the mutual neutralization rate has very similar effects to varying the associative detachment rate, except that the sense of the effect is reversed: a decrease in k_5 has a similar effect to an increase in k_2 and vice versa. The size of the uncertainty introduced into the

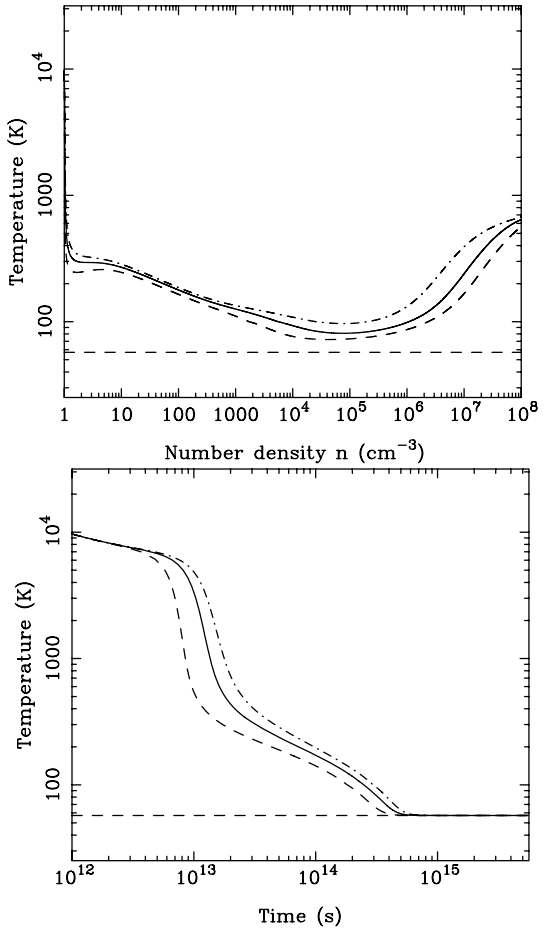

Figure 9. (a) Temperature evolution as a function of gas density for a free-fall collapse model with $n_i = 1\,\mathrm{cm}^{-3}$ and $z = 20$. Three different values are used for the H^- associative detachment rate coefficient (k_2): our default value, taken from Schmeltekopf et al. (1967) (solid line); and 'maximal' and 'minimal' values (dashed and dash–dotted lines, respectively) taken from Glover et al. (2006). The horizontal dashed line indicates the CMB temperature at $z = 20$. (b) As (a), but showing the time evolution of temperature in an isobaric model with the same initial conditions.

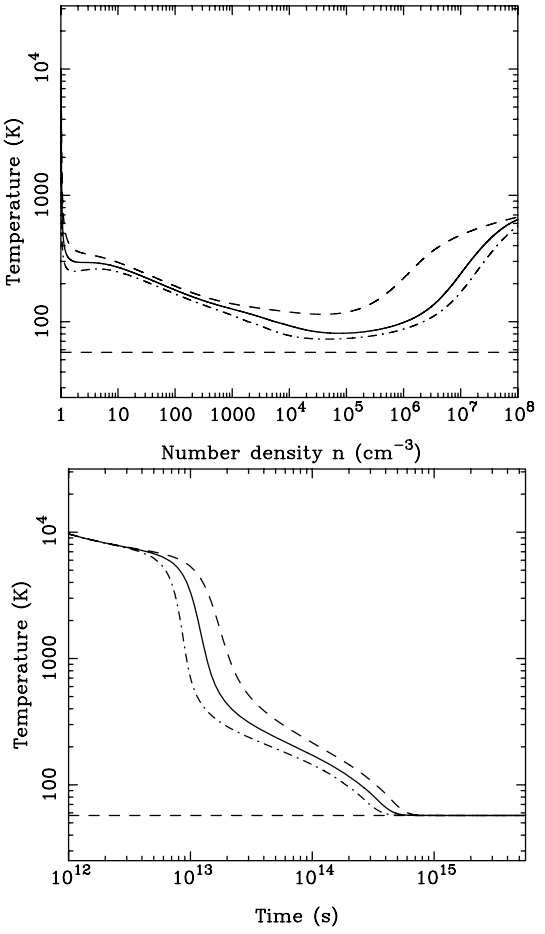

Figure 10. (a) Temperature evolution as a function of gas density for a free-fall collapse model with $n_i = 1\,\mathrm{cm}^{-3}$ and $z = 20$. Three different values are used for the $H^- + H^+$ mutual neutralization rate coefficient (k_5): our default rate (solid line; CDG99), taken from Croft et al. (1999), along with a large rate (dashed line; MOS70), taken from Moseley et al. (1970), and a smaller rate (dash–dotted line; DL87), taken from Dalgarno & Lepp (1987). The horizontal dashed line indicates the CMB temperature at $z = 20$. (b) As (a), but showing the time evolution of temperature in an isobaric model with the same initial conditions.

temperature evolution of the gas is comparable at low densities, and somewhat larger at high densities, where the gas temperatures differ by as much as a factor of 4.

Nevertheless, although both rate coefficient uncertainties clearly affect the cooling of the gas, in neither case do they substantially change the outcome of the simulations. The gas still cools to temperatures low enough for chemical fractionation to significantly enhance HD, and so in each case HD cooling becomes dominant, further cooling the gas. In our free-fall collapse models, the minimum temperature reached by the gas does depend on the values of k_2 and k_5, and this may affect the characteristic fragment mass scale, although we would still expect any fragments to be smaller than in the case where only H_2 cooling is effective. In our isobaric models, the same minimum temperature is reached in every case, but the time taken to arrive there differs by up to a factor of 2. The mass accretion dependent collapse times found by Yoshida et al. (2003) suggest that such a factor of 2 uncertainty can be relevant, but further investigation requires a proper three-dimensional hydrodynamical treatment; our highly simplified dynamical models can take us no further.

3.3.2 H_2 charge transfer

In Fig. 11, we examine the impact of varying the rate coefficient for H_2 destruction by charge transfer (k_7) in the context of representative free-fall collapse and isobaric evolution models. In the free-fall model, the effect of increasing k_7 is to enable the gas to cool to lower temperatures. At first sight, this seems counterintuitive: by destroying H_2, we make the gas colder. However, the key is that charge transfer is only an effective destruction mechanism at high temperatures. By increasing the charge transfer rate, we delay the onset of rapid H_2 cooling, and so when the gas does become able to cool rapidly, the fractional ionization is lower, and the cooling time is longer. Consequently, the gas remains warm for a longer period, forms more H^- (owing to the temperature dependence of reaction 1), and hence forms more H_2. Nevertheless, the effect is relatively small: the uncertainty in the H_2 fraction once the gas has cooled is no more than 5 per cent, and the uncertainty in the minimum temperature is no more than 10 per cent.

In the isobaric model, we again see that the effect of increasing k_7 is to delay the onset of efficient H_2 cooling. However, once the

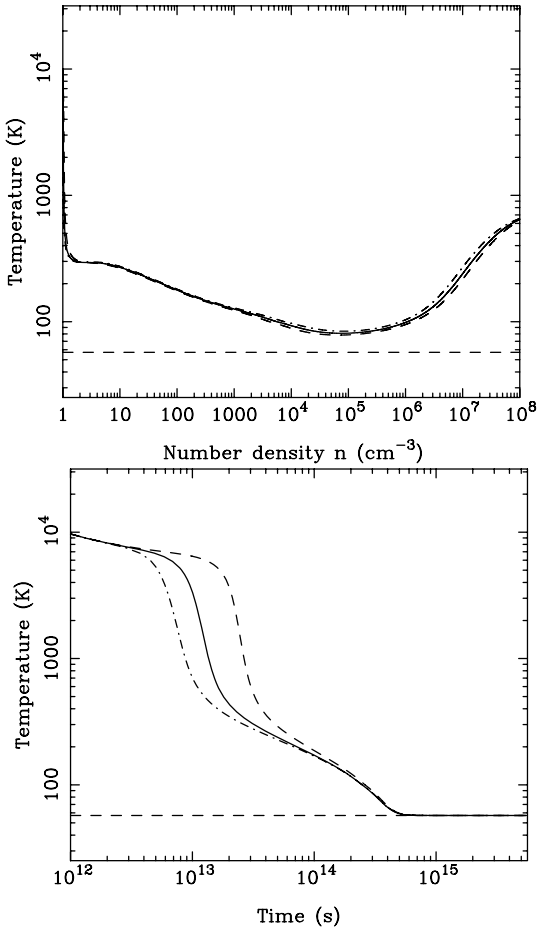

Figure 11. (a) Temperature evolution as a function of gas density for a free-fall collapse model with $n_i = 1\,\mathrm{cm}^{-3}$ and $z = 20$. Three different values are used for the rate coefficient for H_2 destruction by charge transfer with H^+ (reaction 7). The rate used in our reference model (solid line) is taken from Savin et al. (2004), but we also show the effects of using rates from Shapiro & Kang (1987) (dashed line) and Abel et al. (1997) (dash–dotted line). The horizontal dashed line indicates the CMB temperature at $z = 20$. (b) As (a), but showing the time evolution of temperature in an isobaric model with the same initial conditions.

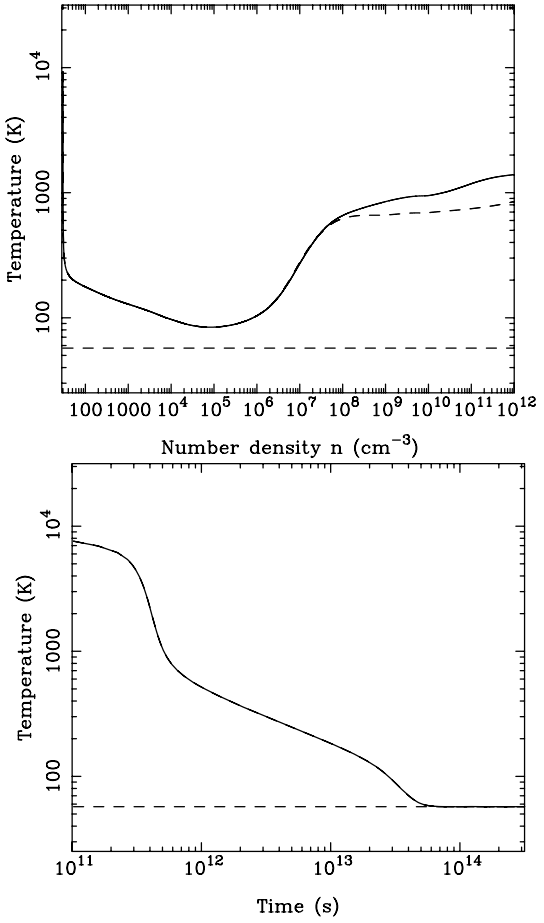

Figure 12. (a) Temperature evolution as a function of gas density in two simulations with $n_i = 30\,\mathrm{cm}^{-3}$ and $z = 20$. Two different values are used for the rate coefficient for three-body H_2 formation (k_{30}): our default value (solid line), taken from Abel et al. (2002), and a much larger value (dashed line) recently computed by Flower & Harris (2007). The horizontal dashed line indicates the CMB temperature at $z = 20$. (b) As (a), but showing the time evolution of temperature in an isobaric model with the same initial conditions. Note that in this plot, the results of the two simulations are indistinguishable.

gas begins cooling, the temperature evolution becomes convergent and the final outcome of the simulations is insensitive to the value of k_7.

3.3.3 Three-body H_2 formation

Since we have assumed, following Palla et al. (1983), that the rate coefficients for reactions (30) and (31) are related by $k_{31} = k_{30}/8$, we can explore the effects of the uncertainty in the three-body rates simply by varying k_{30}. In Fig. 12, we examine the effect of the uncertainty in reaction (30) in two representative models: one free-fall collapse model and one isobaric model.

In the free-fall collapse model, the effect of the uncertainty is apparent only for densities $n > 5 \times 10^6\,\mathrm{cm}^{-3}$. Between this density and $n = 10^8\,\mathrm{cm}^{-3}$, the gas temperature increases slightly faster in the simulation that uses the larger Flower & Harris (2007) rate than in the simulation that uses the smaller Abel et al. (2002) rate, owing to the greater three-body H_2 formation heating rate in the former case. At $n > 10^8\,\mathrm{cm}^{-3}$, however, the greater heating rate in the Flower & Harris run is more than counterbalanced by the greater cooling provided by the larger abundance of H_2, and so the gas temperature increases at a slower rate than in the Abel et al. run. This difference persists until we terminate the simulation at $n = 10^{12}\,\mathrm{cm}^{-3}$, and the final temperatures differ by about 65 per cent.

In the isobaric model, there are no obvious differences between the two simulations. This is to be expected, as the gas density in these simulations never exceeds a few thousand particles per cubic centimetre, and so the three-body H_2 formation rate remains extremely small throughout both simulations.

In neither case does the uncertainty affect the cooling of the gas; in the free-fall model, it merely affects how quickly the gas subsequently reheats. Therefore, whatever its impact on later stages of the star formation process, from the point of view of understanding the role and effectiveness of HD cooling, this particular source of uncertainty is clearly unimportant.

3.3.4 Combining the uncertainties

We close this discussion by examining two limiting cases, illustrated in Fig. 13, where we have selected the values of the various

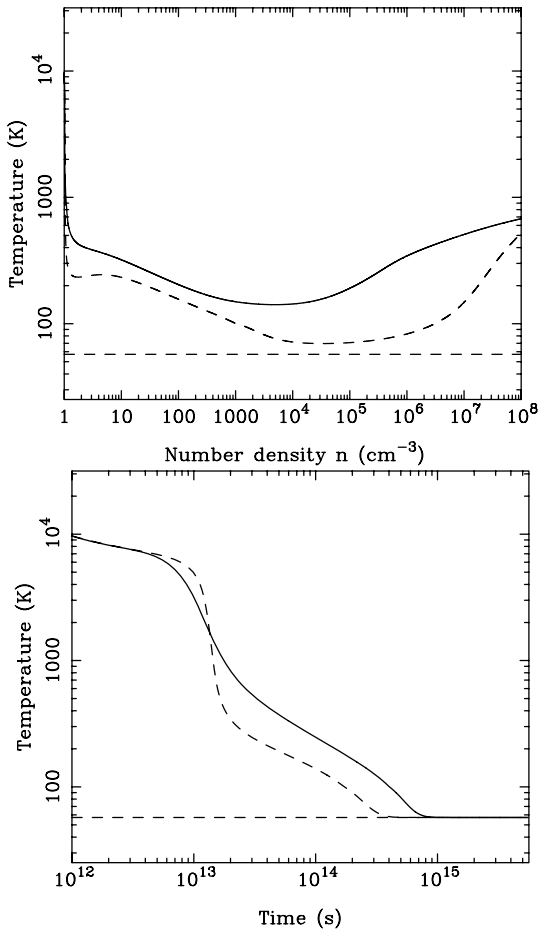

Figure 13. (a) Temperature evolution as a function of gas density in two simulations with $n_i = 1\,\mathrm{cm}^{-3}$ and $z = 20$, with values for the uncertain rate coefficients selected so as to minimize (solid line) or maximize (dashed line) the amount of cooling from H_2. The horizontal dashed line indicates the CMB temperature at $z = 20$. (b) As (a), but showing the time evolution of temperature in an isobaric model with the same initial conditions.

uncertain rate coefficients in order to maximize and to minimize the degree of cooling. In our 'maximal' model, we used a value of $5.0 \times 10^{-9}\,\mathrm{cm}^3\,\mathrm{s}^{-1}$ for the H^- associative detachment rate coefficient (Glover et al. 2006), and used values for the H^- mutual neutralization, H_2 charge transfer and H_2 three-body formation rate coefficients from Dalgarno & Lepp (1987), Abel et al. (1997) and Abel et al. (2002), respectively. In our 'minimal' model, we used a value of $0.65 \times 10^{-9}\,\mathrm{cm}^3\,\mathrm{s}^{-1}$ for the H^- associative detachment rate coefficient (again from Glover et al. 2006), along with values for the other three rate coefficients taken from Moseley et al. (1970), Shapiro & Kang (1987) and Flower & Harris (2007), respectively. Note that in both models, the Wrathmall & Flower (2007) H_2 cooling rate is used and the effects of cooling from H_2–H_2, H_2–He, H_2–H^+ and H_2–e^- collisions are included; i.e. we do not couple the chemical rate uncertainties to the cooling rate uncertainties.

In Fig. 13(a), we examine the effects of the 'minimal' and 'maximal' models in the context of a representative free-fall collapse calculation with an initial redshift $z = 20$. The temperature evolution in the two models differs significantly at all densities, particularly in the interval $10^4 < n < 10^8\,\mathrm{cm}^{-3}$. The minimum temperature reached by the gas in the 'maximal' model is 69.8 K, and in the 'minimal' model is 141.5 K, a factor of 2 difference (corresponding to a difference in the Jeans mass at this point of almost a factor of 3). It is clear that in the 'minimal' model, HD cooling is of limited importance: although some HD cooling does occur, it never becomes completely dominant, and the gas temperature remains well above the floor set by the CMB. If the rates adopted in this model do prove to be the most accurate ones, then this would imply that HD cooling in collapsing gas may be significantly less effective than previously thought.

Finally, in Fig. 13(b), we examine the effects of the 'minimal' and 'maximal' models in the context of an isobaric evolution model with an initial redshift $z = 20$. Again, we see that the rate coefficient uncertainties significantly affect the cooling time of the gas, lengthening it in this case by a factor of 3. However, they do not change the final outcome of the simulation: the gas still cools down to $T \sim T_{\mathrm{CMB}}$, and even for the 'minimal' model, the time required to reach T_{CMB} when $n_i = 1\,\mathrm{cm}^{-3}$ is significantly less than a Hubble time.

4 SUMMARY

We have detailed the effect of several possible sources of uncertainty on the thermal evolution of primordial gas cooling from an initially hot and ionized state. These considered potential sources of uncertainty are the sensitivity of the low-temperature H_2 cooling rate to the ratio of ortho-H_2 to para-H_2 (which may differ significantly at low temperatures from the 3:1 ratio that is usually assumed), the continuing uncertainty in the form of the low-temperature cooling rate for H_2 excited by collisions with atomic hydrogen, the neglect by most previous authors of the contributions made to the H_2 cooling rate by collisions of H_2 with He, H^+ and e^-, and the large uncertainties that exist in the rates of several of the reactions responsible for determining the H_2 fraction in the gas.

We find that the first of these sources of uncertainty is unimportant. The standard assumption of a 3:1 ortho–para ratio is reasonably accurate at temperatures where H_2 cooling is effective. It only becomes significantly inaccurate for temperatures $T \lesssim 100\,\mathrm{K}$, but at these temperatures H_2 cooling is unimportant in comparison to HD cooling, and so this inaccuracy has no effect on the thermal evolution of the gas. However, the presented rates and formalism should prove useful when detailed complete emission models from cooling primordial gas are to be constructed.

The second source of uncertainty – i.e. whether one uses the popular Galli & Palla (1998) parameterization to represent the cooling rate due to H_2–H collisions, or the newer rates of Wrathmall & Flower (2007) – can give the impression of being important if one assumes that this process dominates the total H_2 cooling rate. At low temperatures ($T < 1000\,\mathrm{K}$), the Wrathmall & Flower (2007) cooling function provides significantly less cooling than the Galli & Palla (1998) cooling function, and the use of the former in place of the latter lengthens the cooling time of the gas by about a factor of 2.

However, this simple comparison overstates the effect of this uncertainty. The problem stems from the assumption that H_2–H collisions dominate. In practice, if one adopts the Wrathmall & Flower (2007) cooling rate, then at low temperatures, H_2–He collisions are more important, despite the low abundance of He relative to H. If one includes the effects of these collisions in the calculations, then the sensitivity of the outcome to the uncertainty in the H_2–H rate becomes considerably less.

A more important source of error in previous investigations of HD formation in relic H II regions and other similar environments is the neglect of the effects of cooling due to collisions between H_2 and protons and electrons. At early times during the cooling of the

gas, the fractional ionization remains large, and H_2–H^+ collisions dominate. When their effects are included, the cooling time of the gas is significantly decreased. However, a side effect of this rapid cooling is that less H_2 forms, owing to the temperature dependence of the H_2 formation rate. Because of this, less HD is formed, and so HD cooling is less effective. Therefore, the gas remains significantly warmer at later times than it would in models that did not include cooling from H_2–H^+ collisions, although it remains cooler than it would be if HD cooling were not included. The increase in the minimum temperature in our free-fall models corresponds to an increase in the minimum Jeans mass of a factor of 2, suggesting that previous studies of Population III star formation in formerly ionized regions may have underestimated the characteristic mass of the stars that form. Moreover, previous work by Yoshida et al. (2003) has shown that variations in the cooling time of the gas at low densities can have a pronounced effect on the supply of cold gas available for Population III star formation, and on the timing of the collapse. Furthermore, O'Shea & Norman (2007) have shown that the amount of H_2 formed at low densities, which is sensitive to the thermal evolution of the gas, can affect the eventual accretion rate of gas on to the protostar, and hence may also affect its final mass. We therefore anticipate that the inclusion of the effects of H_2–H^+ cooling may lead to clear differences in the outcome of such three-dimensional studies.

Our investigation into the effects of the chemical rate coefficient uncertainties has shown that the large uncertainties in the associative detachment and mutual neutralization rates also have a significant impact on the thermal evolution of the gas. Although HD becomes the dominant coolant in all of the models considered, variations in the associative detachment and mutual neutralization rates alter the minimum temperature reached by the gas in our free-fall collapse simulations, and have a particularly pronounced effect on the temperature evolution at the end of the period during which HD cooling dominates. It is therefore quite plausible that these uncertainties may also modify the outcome of multidimensional hydrodynamical simulations.

On the other hand, our results display only a small sensitivity to the uncertainty in the H_2 charge transfer reaction, other than at very early times in the isobaric runs, due to the fact that most of the H_2 that forms in the gas does so at temperatures where this reaction is ineffective. Further investigation of the effects of this uncertainty may be of interest, but is clearly not a high priority.

Finally, our results demonstrate that the evolution of gas in the HD-cooled regime is insensitive to the large uncertainty that exists in the three-body H_2 formation rate, as three-body processes are unimportant at the densities at which HD dominates. However, this uncertainty does become important at densities $n > 10^8\,\mathrm{cm}^{-3}$. Its effect on the hydrodynamics of the gas at these densities remains uncertain.

In summary, we discussed a number of hitherto neglected physical processes. The most crucial finding is that the molecular hydrogen cooling initiated by collisions with electrons, protons and neutral helium cannot be neglected in general, and should be included in future studies of the dynamics of primordial gas.

ACKNOWLEDGMENTS

The authors would like to thank D. Galli for discussions concerning H_2^+ cooling, and for kindly providing to us the fit given in equation (47). They would also like to thank A. Dalgarno, N. Yoshida, D. Whalen and the anonymous referee for their comments on an earlier draft of this article. In particular, the referee deserves thanks for pointing out to us the possible importance of cooling from collisions between molecular hydrogen and helium. SCOG acknowledges useful discussions with D. Savin and P. Stancil regarding the rate of reactions involving deuterium. Financial support was provided in part by the US National Science Foundation under Grant No. PHY05-51164, and by NSF CAREER award AST-0239709. This project was initiated while the authors were participants in the workshop 'Star Formation Through Cosmic Time' at the Kavli Institute for Theoretical Physics, and we thank the staff and scholars of KITP for their hospitality.

REFERENCES

Abel T., Anninos P., Zhang Y., Norman M. L., 1997, New Astron., 2, 181
Abel T., Bryan G. L., Norman M. L., 2002, Sci, 295, 93
Abgrall H., Roueff E., Viala Y., 1982, A&AS, 50, 505
Aldrovandi S. M. V., Pequignot D., 1973, A&A, 25, 137
Balakrishnan N., Forrey R. C., Dalgarno A., 1999a, ApJ, 514, 520
Balakrishnan N., Viera M., Babb J. F., Dalgarno A., Forrey R. C., Lepp S., 1999b, ApJ, 524, 1122
Barlow S. G., 1984, PhD thesis, Univ. Colorado
Boothroyd A. I., Keogh W. J., Martin P. G., Peterson M. R., 1996, J. Chem. Phys., 104, 7139
Boothroyd A. I., Martin P. G., Peterson M. R., 2003, J. Chem. Phys., 119, 3187
Bray I., Burgess A., Fursa D. V., Tully J. A., 2000, A&AS, 148, 481
Bromm V., Larson R. B., 2004, ARA&A, 42, 79
Bromm V., Coppi P. S., Larson R. B., 2002, ApJ, 564, 23
Brown P. N., Byrne G. D., Hindmarsh A. C., 1989, SIAM J. Sci. Stat. Comput., 10, 1038
Cen R., 1992, ApJS, 78, 341
Clark P. C., Glover S. C. O., Klessen R. S., 2008, ApJ, 672, 757
Croft H., Dickinson A. S., Gadea F. X., 1999, MNRAS, 304, 327
Crompton R. W., Gibson D. K., McIntosh A. I., 1969, Aust. J. Phys., 22, 715
Dalgarno A., Lepp S., 1987, in Vardya M. S., Tarafdar S. P., eds, Astrochemistry. Reidel, Dordrecht, p. 109
Dalgarno A., McDowell M. R. C., 1956, Proc. Phys. Soc. London A, 69, 615
Dickinson A. S., 2005, J. Phys. B, 38, 4329
Dove J. E., Rusk A. C. M., Cribb P. H., Martin P. G., 1987, ApJ, 318, 379
Draine B. T., Roberge W. G., Dalgarno A., 1983, ApJ, 264, 485
Ehrhardt H., Langhans L., Linder F., Taylor H. S., 1968, Phys. Rev., 173, 222
Ferland G. J., Peterson B. M., Horne K., Welsh W. F., Nahar S. N., 1992, ApJ, 387, 95
Flower D. R., Harris G. J., 2007, MNRAS, 377, 705
Flower D. R., Roueff E., 1998, J. Phys. B, 31, 2935
Flower D. R., Roueff E., 1999, J. Phys. B, 32, 3399
Flower D. R., Roueff E., Zeippen C. J., 1998, J. Phys. B, 31, 1105
Flower D. R., Le Bourlot J., Pineau des Forêts G., Roueff E., 2000a, MNRAS, 314, 753
Flower D. R., Pineau des Forêts G., 2000b, MNRAS, 316, 901
Forrey R. C., Balakrishnan N., Dalgarno A., Lepp S., 1997, ApJ, 489, 1000
Galli D., Palla F., 1998, A&A, 335, 403
Gerlich D., 1982, in Lindinger W., Howorka F., Märk T. D., eds, Symposium on Atomic and Surface Physics. Kluwer, Dordrecht, p. 304
Gerlich D., 1990, J. Chem. Phys., 92, 2377
Glover S. C. O., 2005, Space Sci. Rev., 117, 445
Glover S. C. O., 2008, in O'Shea B., Heger A., Abel T., eds, First Stars III. Am. Inst. Phys., New York, p. 25
Glover S. C. O., Jappsen A.-K., 2007, ApJ, 666, 1
Glover S. C. O., Savin D. W., 2006, Phil. Trans. R. Soc. London A, 364, 3107
Glover S. C. O., Savin D. W., Jappsen A.-K., 2006, ApJ, 640, 553
Hummer D. G., Storey P. J., 1998, MNRAS, 297, 1073

Huq M. S., Doverspike L. D., Champion R. L., Esaulov V. A., 1982, J. Phys. B, 15, 951
Janev R. K., Langer W. D., Evans K., Post D. E., 1987, Elementary Processes in Hydrogen–Helium Plasmas. Springer-Verlag, Berlin
Jasche J., Ciardi B., Ensslin T. A., 2007, MNRAS, 380, 417
Johnson J. L., Bromm V., 2006, MNRAS, 366, 247
Johnson J. L., Greif T. H., Bromm V., 2007, ApJ, 665, 85
Karpas Z., Anicich V., Huntress W. T., 1979, J. Chem. Phys., 70, 2877
Karr J. Ph., Hilico L., 2006, J. Phys. B, 39, 2095
Kimura M., Lane N. F., Dalgarno A., Dixson R. G., 1993, ApJ, 405, 801
Krstić P. S., 2002, Phys. Rev. A, 66, 042717
Launay J. M., Le Dourneuf M., Zeippen C. J., 1991, A&A, 252, 842
Le Bourlot J., Pineau des Forêts G., Flower D. R., 1999, MNRAS, 305, 802
Lee T.-G. et al., 2005, J. Chem. Phys., 122, 024307
Lepp S., Shull J. M., 1983, ApJ, 270, 578
Linder F., Schmidt H., 1971, Z. Naturf., 26a, 1603
Linder F., Janev R. K., Botero J., 1995, in Janev R. K., ed., Atomic and Molecular Processes in Fusion Edge Plasmas. Plenum Press, New York, p. 397
Lipovka A., Núñez-López R., Avila-Reese V., 2005, MNRAS, 361, 850
Liu B., 1973, J. Chem. Phys., 58, 1925
Mac Low M.-M., Shull J. M., 1986, ApJ, 302, 585
Mandy M. E., Martin P. G., 1993, ApJS, 86, 199
Martin P. G., Schwarz D. H., Mandy M. E., 1996, ApJ, 461, 265
Martin P. G., Keogh W. J., Mandy M. E., 1998, ApJ, 499, 793
Mielke S. L., Garrett B. C., Peterson K. A., 2002, J. Chem. Phys., 116, 4142
Mielke S. L., Peterson K. A., Schwenke D. W., Garrett B. C., Truhlar D. G., Michael J. V., Su M.-C., Sutherland J. W., 2003, Phys. Rev. Lett., 91, 063201
Molaro P., 2007, preprint (arXiv:0708.3922)
Moseley J., Aberth W., Peterson J. R., 1970, Phys. Rev. Lett., 24, 435
Muchnick P., Russek A., 1994, J. Chem. Phys., 100, 4336
Nagakura T., Omukai K., 2005, MNRAS, 364, 1378
Nakamura F., Umemura, M., 2002, ApJ, 569, 549
Orel A. E., 1987, J. Chem. Phys., 87, 314
O'Shea B. W., Norman M. L., 2007, ApJ, 654, 66
O'Shea B. W., Abel T., Whalen D., Norman M. L., 2005, ApJ, 628, L5
Osterbrock D. E., 1989, Astrophysics of Gaseous Nebulae and Active Galactic Nuclei. University Science Books, Mill Valley, CA
Palla F., Salpeter E. E., Stahler S. W., 1983, ApJ, 271, 632
Peart B., Hayton D. A., 1994, J. Phys. B, 27, 2551
Peek J. M., Hashemi-Attar A.-R., Beckel C. L., 1979, J. Chem. Phys., 71, 5382
Posen A. G., Dalgarno A., Peek J. M., 1983, At. Data Nucl. Data Tables, 28, 265
Poulaert G., Brouillard F., Claeys W., McGowan J. W., Van Wassenhove G., 1978, J. Phys. B, 11, L671
Ramaker D. E., Peek J. M., 1976, Phys. Rev. A, 13, 58
Santoro F., Shull J. M., 2006, ApJ, 643, 26
Sarpal B. K., Tennyson J., 1993, MNRAS, 263, 909
Savin D. W., 2002, ApJ, 566, 599
Savin D. W., Krstic P. S., Haiman Z., Stancil P. C., 2004, ApJ, 606, L167 (erratum: ApJ, 607, L147)
Schmeltekopf A. L., Fehsenfeld F. C., Ferguson E. E., 1967, ApJ, 118, L155
Schneider I. F., Dulieu O., Giusti-Suzor A., Roueff E., 1994, ApJ, 424, 983 (erratum: ApJ, 486, 580)
Schulz G. J., Asundi R. K., 1967, Phys. Rev., 158, 25
Shapiro P. R., Kang H., 1987, ApJ, 318, 32
Shavitt I., 1959, J. Chem. Phys., 31, 1359
Shchekinov Y. A., Vasiliev E. O., 2004, A&A, 419, 19
Shchekinov Y. A., Vasiliev E. O., 2006, MNRAS, 368, 454
Siegbahn P., Liu B., 1978, J. Chem. Phys., 68, 2457
Spergel D. N. et al., 2007, ApJS, 170, 377
Stacy A., Bromm V., 2007, MNRAS, 382, 229
Stancil P. C., Lepp S., Dalgarno A., 1998, ApJ, 509, 1
Stromhölm C., Schneider I. F., Sundström G. et al., 1995, Phys. Rev. A, 52, R4320
Suchkov A. A., Shchekinov, Yu. A., 1978, Sov. Astron. Lett., 4, 164
Sun Y., Dalgarno A., 1994, ApJ, 427, 1053
Trevisan C. S., Tennyson J., 2002a, Plasma Phys. Control. Fusion, 44, 1263
Trevisan C. S., Tennyson J., 2002b, Plasma Phys. Control. Fusion, 44, 2217
Truhlar D. G., Horowitz C. J., 1978, J. Chem. Phys., 68, 2466
Vasiliev E. O., Shchekinov Y. A., 2006, Astron. Rep., 50, 778
Walkauskas L. P., Kaufman F., 1975, Symp. Int. Combust. Proc., 15, 691
Walmsley C. M., Flower D. R., Pineau des Forêts G., 2004, A&A, 418, 1035
Wang J. G., Stancil P. C., 2002, Phys. Scr., T96, 72
Wishart A. W., 1979, MNRAS, 187, 59P
Wolniewicz L., Simbotin I., Dalgarno A., 1998, ApJS, 115, 293
Wrathmall S. A., Flower D. R., 2007, J. Phys. B, 40, 3221
Wrathmall S. A., Gusdorf A., Flower D. R., 2007, MNRAS, 382, 133
Xu Y., Fabrikant I. I., 2001, Appl. Phys. Lett., 78, 2598
Yoshida N., Abel T., Hernquist L., Sugiyama N., 2003, ApJ, 592, 645
Yoshida N., Omukai K., Hernquist L., Abel T., 2006, ApJ, 652, 6
Yoshida N., Oh S. P., Kitayama T., Hernquist L., 2007, ApJ, 663, 687
Zygelman B., Dalgarno A., Kimura M., Lane N. F., 1989, Phys. Rev. A, 40, 2340

APPENDIX A: CHEMICAL NETWORK

In Table A1 we list the chemical reactions included in our model of primordial gas, along with the rate coefficients adopted and the references from which these rates were taken. For further details on some of the reactions, see also Section 2.1.

Table A1. List of reactions included in our chemical model.

No.	Reaction	Rate coefficient ($cm^3\ s^{-1}$)		Reference
1	$H + e^- \rightarrow H^- + \gamma$	$k_1 = \mathrm{dex}[-17.845 + 0.762 \log T$ $+0.1523\ (\log T)^2$ $-0.032\,74\ (\log T)^3]$	$T \leqslant 6000\,K$	1
		$-\mathrm{dex}[-16.4199 + 0.1998\ (\log T)^2$ $-5.447 \times 10^{-3}\ (\log T)^4$ $+4.0415 \times 10^{-5}\ (\log T)^6]$	$T > 6000\,K$	
2	$H^- + H \rightarrow H_2 + e^-$	See text		–
3	$H + H^+ \rightarrow H_2^+ + \gamma$	$k_3 = \mathrm{dex}[-19.38 - 1.523 \log T$ $+1.118\ (\log T)^2 - 0.1269\ (\log T)^3]$		2
4	$H + H_2^+ \rightarrow H_2 + H^+$	$k_4 = 6.4 \times 10^{-10}$		3
5	$H^- + H^+ \rightarrow H + H$	See text		–
6	$H_2^+ + e^- \rightarrow H + H$	$k_6 = 1.0 \times 10^{-8}$	$T \leqslant 617\,K$	4
		$= 1.32 \times 10^{-6}\ T^{-0.76}$	$T > 617\,K$	
7	$H_2 + H^+ \rightarrow H_2^+ + H$	$k_7 = [-3.323\,2183 \times 10^{-7}$ $+3.373\,5382 \times 10^{-7} \log T$ $-1.449\,1368 \times 10^{-7}\ (\log T)^2$ $+3.417\,2805 \times 10^{-8}\ (\log T)^3$ $-4.781\,3720 \times 10^{-9}\ (\log T)^4$ $+3.973\,1542 \times 10^{-10}\ (\log T)^5$ $-1.817\,1411 \times 10^{-11}\ (\log T)^6$ $+3.531\,1932 \times 10^{-13}\ (\log T)^7]$ $\times \exp\left(\frac{-21\,237.15}{T}\right)$		5
8	$H_2 + e^- \rightarrow H + H + e^-$	$k_8 = 4.49 \times 10^{-9} T^{0.11} \exp\left(-\frac{101\,858}{T}\right)$	$v = 0$	6
		$= 1.91 \times 10^{-9} T^{0.136} \exp\left(-\frac{53\,407.1}{T}\right)$	LTE	6
9	$H_2 + H \rightarrow H + H + H$	$k_9 = 6.67 \times 10^{-12} T^{0.5} \exp\left[-\left(1 + \frac{63\,593}{T}\right)\right]$	$v = 0$	7
		$= 3.52 \times 10^{-9} \exp\left(-\frac{43\,900}{T}\right)$	LTE	8
10	$H_2 + H_2 \rightarrow H_2 + H + H$	$k_{10} = \frac{5.996 \times 10^{-30} T^{4.1881}}{(1.0 + 6.761 \times 10^{-6} T)^{5.6881}} \exp\left(-\frac{54\,657.4}{T}\right)$	$v = 0$	9
		$= 1.3 \times 10^{-9} \exp\left(-\frac{53\,300}{T}\right)$	LTE	10
11	$H_2 + He \rightarrow H + H + He$	$k_{11} = \mathrm{dex}\left[-27.029 + 3.801 \log T - \frac{29\,487}{T}\right]$	$v = 0$	11
		$= \mathrm{dex}\left[-2.729 - 1.75 \log T - \frac{23\,474}{T}\right]$	LTE	11
12	$H + e^- \rightarrow H^+ + e^- + e^-$	$k_{12} = \exp[-3.271\,396\,786 \times 10^1$ $+1.353\,655\,60 \times 10^1 \ln T_e$ $-5.739\,328\,75 \times 10^0\ (\ln T_e)^2$ $+1.563\,154\,98 \times 10^0\ (\ln T_e)^3$ $-2.877\,056\,00 \times 10^{-1}\ (\ln T_e)^4$ $+3.482\,559\,77 \times 10^{-2}\ (\ln T_e)^5$ $-2.631\,976\,17 \times 10^{-3}\ (\ln T_e)^6$ $+1.119\,543\,95 \times 10^{-4}\ (\ln T_e)^7$ $-2.039\,149\,85 \times 10^{-6}\ (\ln T_e)^8]$		12
13	$H^+ + e^- \rightarrow H + \gamma$	$k_{13,A} = 1.269 \times 10^{-13} \left(\frac{315\,614}{T}\right)^{1.503}$ $\times \left[1.0 + \left(\frac{604\,625}{T}\right)^{0.470}\right]^{-1.923}$	Case A	13
		$k_{13,B} = 2.753 \times 10^{-14} \left(\frac{315\,614}{T}\right)^{1.500}$ $\times \left[1.0 + \left(\frac{115\,188}{T}\right)^{0.407}\right]^{-2.242}$	Case B	13
14	$H^- + e^- \rightarrow H + e^- + e^-$	$k_{14} = \exp\left[-1.801\,849\,334 \times 10^1\right.$ $+2.360\,852\,20 \times 10^0 \ln T_e$ $-2.827\,443\,00 \times 10^{-1}\ (\ln T_e)^2$ $+1.623\,316\,64 \times 10^{-2}\ (\ln T_e)^3$ $-3.365\,012\,03 \times 10^{-2}\ (\ln T_e)^4$ $+1.178\,329\,78 \times 10^{-2}\ (\ln T_e)^5$ $-1.656\,194\,70 \times 10^{-3}\ (\ln T_e)^6$ $+1.068\,275\,20 \times 10^{-4}\ (\ln T_e)^7$ $\left.-2.631\,285\,81 \times 10^{-6}\ (\ln T_e)^8\right]$		12

Table A1 – *continued*

No.	Reaction	Rate coefficient ($cm^3\ s^{-1}$)		Reference
15	$H^- + H \rightarrow H + H + e^-$	$k_{15} = 2.5634 \times 10^{-9} T_e^{1.781\,86}$	$T_e \leqslant 0.1$ eV	12
		$= \exp[-2.037\,2609 \times 10^{1}$	$T_e > 0.1$ eV	
		$+1.139\,449\,33 \times 10^{0} \ln T_e$		
		$-1.421\,0135 \times 10^{-1} (\ln T_e)^2$		
		$+8.464\,4554 \times 10^{-3} (\ln T_e)^3$		
		$-1.432\,7641 \times 10^{-3} (\ln T_e)^4$		
		$+2.012\,2503 \times 10^{-4} (\ln T_e)^5$		
		$+8.663\,9632 \times 10^{-5} (\ln T_e)^6$		
		$-2.585\,0097 \times 10^{-5} (\ln T_e)^7$		
		$+2.455\,5012 \times 10^{-6} (\ln T_e)^8$		
		$-8.068\,3825 \times 10^{-8} (\ln T_e)^9]$		
16	$H^+ + H^- \rightarrow H_2^+ + e^-$	$k_{16} = 6.9 \times 10^{-9}\ T^{-0.35}$	$T \leqslant 8000$ K	14
		$= 9.6 \times 10^{-7}\ T^{-0.90}$	$T > 8000$ K	
17	$He + e^- \rightarrow He^+ + e^- + e^-$	$k_{17} = \exp[-4.409\,864\,886 \times 10^{1}$		12
		$+2.391\,596\,563 \times 10^{1} \ln T_e$		
		$-1.075\,323\,02 \times 10^{1} (\ln T_e)^2$		
		$+3.058\,038\,75 \times 10^{0} (\ln T_e)^3$		
		$-5.685\,118\,90 \times 10^{-1} (\ln T_e)^4$		
		$+6.795\,391\,23 \times 10^{-2} (\ln T_e)^5$		
		$-5.009\,056\,10 \times 10^{-3} (\ln T_e)^6$		
		$+2.067\,236\,16 \times 10^{-4} (\ln T_e)^7$		
		$-3.649\,161\,41 \times 10^{-6} (\ln T_e)^8]$		
18	$He^+ + e^- \rightarrow He^{++} + e^- + e^-$	$k_{18} = \exp[-6.871\,040\,99 \times 10^{1}$		12
		$+4.393\,347\,633 \times 10^{1} \ln T_e$		
		$-1.848\,066\,99 \times 10^{1} (\ln T_e)^2$		
		$+4.701\,626\,49 \times 10^{0} (\ln T_e)^3$		
		$-7.692\,4663 \times 10^{-1} (\ln T_e)^4$		
		$+8.113\,042 \times 10^{-2} (\ln T_e)^5$		
		$-5.324\,020\,63 \times 10^{-3} (\ln T_e)^6$		
		$+1.975\,705\,31 \times 10^{-4} (\ln T_e)^7$		
		$-3.165\,581\,06 \times 10^{-6} (\ln T_e)^8]$		
19	$He^+ + e^- \rightarrow He + \gamma$	$k_{19,rr,A} = 10^{-11}\ T^{-0.5}\ [12.72 - 1.615 \log T$	Case A	15
		$-0.3162 (\log T)^2 + 0.0493 (\log T)^3]$		
		$k_{19,rr,B} = 10^{-11}\ T^{-0.5}\ [11.19 - 1.676 \log T$	Case B	15
		$-0.2852 (\log T)^2 + 0.044\,33 (\log T)^3]$		
		$k_{19,di} = 1.9 \times 10^{-3} T^{-1.5} \exp\left(-\frac{473\,421}{T}\right)$	Dielectronic	16
		$\times \left[1.0 + 0.3 \exp\left(-\frac{94\,684}{T}\right)\right]$		
20	$He^{++} + e^- \rightarrow He^+ + \gamma$	$k_{20,A} = 2.538 \times 10^{-13} \left(\frac{1262\,456}{T}\right)^{1.503}$	Case A	13
		$\times \left[1.0 + \left(\frac{2418\,500}{T}\right)^{0.470}\right]^{-1.923}$		
		$k_{20,B} = 5.506 \times 10^{-14} \left(\frac{1262\,456}{T}\right)^{1.500}$	Case B	13
		$\times \left[1.0 + \left(\frac{460\,752}{T}\right)^{0.407}\right]^{-2.242}$		
21	$H^- + H_2^+ \rightarrow H_2 + H$	$k_{21} = 1.4 \times 10^{-7} \left(\frac{T}{300}\right)^{-0.5}$		17
22	$H^- + H_2^+ \rightarrow H + H + H$	$k_{22} = 1.4 \times 10^{-7} \left(\frac{T}{300}\right)^{-0.5}$		17
23	$H_2 + e^- \rightarrow H^- + H$	$k_{23} = 2.7 \times 10^{-8} T^{-1.27} \exp\left(-\frac{43\,000}{T}\right)$		18
24	$H_2 + He^+ \rightarrow He + H + H^+$	$k_{24} = 3.7 \times 10^{-14} \exp\left(\frac{35}{T}\right)$		19
25	$H_2 + He^+ \rightarrow H_2^+ + He$	$k_{25} = 7.2 \times 10^{-15}$		19
26	$He^+ + H \rightarrow He + H^+$	$k_{26} = 1.2 \times 10^{-15} \left(\frac{T}{300}\right)^{0.25}$		20
27	$He + H^+ \rightarrow He^+ + H$	$k_{27} = 1.26 \times 10^{-9} T^{-0.75} \exp\left(-\frac{127\,500}{T}\right)$	$T \leqslant 10\,000$ K	21
		$= 4.0 \times 10^{-37}\ T^{4.74}$	$T > 10\,000$ K	
28	$He^+ + H^- \rightarrow He + H$	$k_{28} = 2.32 \times 10^{-7} \left(\frac{T}{300}\right)^{-0.52} \exp\left(\frac{T}{22\,400}\right)$		22
29	$He + H^- \rightarrow He + H + e^-$	$k_{29} = 4.1 \times 10^{-17} T^2 \exp\left(-\frac{19\,870}{T}\right)$		23
30	$H + H + H \rightarrow H_2 + H$	See text		–
31	$H + H + H_2 \rightarrow H_2 + H_2$	See text		–
32	$H + H + He \rightarrow H_2 + He$	$k_{32} = 6.9 \times 10^{-32}\ T^{-0.4}$		24
33	$D^+ + e^- \rightarrow D + \gamma$	$k_{33} = k_{13}$		25

Table A1 – *continued*

No.	Reaction	Rate coefficient ($cm^3\ s^{-1}$)		Reference
34	$D + H^+ \rightarrow H + D^+$	$k_{34} = 2.0 \times 10^{-10} T^{0.402} \exp\left(-\frac{37.1}{T}\right)$	$T \leqslant 2 \times 10^5$ K	26
		$-3.31 \times 10^{-17}\ T^{1.48}$		
		$= 3.44 \times 10^{-10}\ T^{0.35}$	$T > 2 \times 10^5$ K	
35	$H + D^+ \rightarrow D + H^+$	$k_{35} = 2.06 \times 10^{-10} T^{0.396} \exp\left(-\frac{33}{T}\right)$		26
		$+2.03 \times 10^{-9}\ T^{-0.332}$		
36	$H + D \rightarrow HD + \gamma$	$k_{36} = 10^{-25}\ [2.802\,02 - 6.636\,97 \ln T$	$10 < T \leqslant 200$ K	27
		$+4.756\,19\ (\ln T)^2 - 1.393\,25\ (\ln T)^3$		
		$+0.178\,259\ (\ln T)^4 - 0.008\,170\,97\ (\ln T)^5]$		
		$= 10^{-25} \exp\ [507.207 - 370.889 \ln T$	$T > 200$ K	
		$+104.854\ (\ln T)^2 - 14.4192\ (\ln T)^3$		
		$+0.971\,469\ (\ln T)^4 - 0.025\,8076\ (\ln T)^5]$		
37	$H_2 + D \rightarrow HD + H$	$k_{37} = \mathrm{dex}[-56.4737 + 5.888\,86 \log T$	$T \leqslant 2000$ K	28
		$+7.196\,92\ (\log T)^2$		
		$+2.250\,69\ (\log T)^3$		
		$-2.169\,03\ (\log T)^4$		
		$+0.317\,887\ (\log T)^5]$		
		$= 3.17 \times 10^{-10} \exp\left(-\frac{5207}{T}\right)$	$T > 2000$ K	
38	$HD^+ + H \rightarrow HD + H^+$	$k_{38} = k_4$		25
39	$H_2 + D^+ \rightarrow HD + H^+$	$k_{39} = [0.417 + 0.846 \log T - 0.137\ (\log T)^2] \times 10^{-9}$		29
40	$HD + H \rightarrow H_2 + D$	$k_{40} = 5.25 \times 10^{-11} \exp\left(-\frac{4430}{T}\right)$	$T \leqslant 200$ K	30
		$= 5.25 \times 10^{-11} \exp\left(-\frac{4430}{T} + \frac{173\,900}{T^2}\right)$	$T > 200$ K	
41	$HD + H^+ \rightarrow H_2 + D^+$	$k_{41} = 1.1 \times 10^{-9} \exp\left(-\frac{488}{T}\right)$		29
42	$D + H^+ \rightarrow HD^+ + \gamma$	$k_{42} = 3.9 \times 10^{-19} \left(\frac{T}{300}\right)^{1.8} \exp\left(\frac{20}{T}\right)$		31
43	$H + D^+ \rightarrow HD^+ + \gamma$	$k_{43} = 3.9 \times 10^{-19} \left(\frac{T}{300}\right)^{1.8} \exp\left(\frac{20}{T}\right)$		31
44	$HD^+ + e^- \rightarrow H + D$	$k_{44} = 7.2 \times 10^{-8}\ T^{-0.5}$		32
45	$D + e^- \rightarrow D^+ + e^- + e^-$	$k_{45} = k_{12}$		25
46	$He^+ + D \rightarrow D^+ + He$	$k_{46} = 1.1 \times 10^{-15} \left(\frac{T}{300}\right)^{0.25}$		31
47	$He + D^+ \rightarrow D + He^+$	$k_{47} = 1.85 \times 10^{-9} T^{-0.75} \exp\left(-\frac{127\,500}{T}\right)$	$T \leqslant 10\,000$ K	31
		$= 5.9 \times 10^{-37}\ T^{4.74}$	$T > 10\,000$ K	
48	$H_2^+ + D \rightarrow HD^+ + H$	$k_{48} = 1.07 \times 10^{-9} \left(\frac{T}{300}\right)^{0.062} \exp\left(-\frac{T}{41\,400}\right)$		33
49	$HD^+ + D \rightarrow HD + D^+$	$k_{49} = k_4$		25
50	$HD^+ + H \rightarrow H_2^+ + D$	$k_{50} = 1.0 \times 10^{-9} \exp\left(-\frac{154}{T}\right)$		34
51	$D + e^- \rightarrow D^- + \gamma$	$k_{51} = k_1$		25
52	$H + D^- \rightarrow D + H^-$	$k_{52} = 6.4 \times 10^{-9} \left(\frac{T}{300}\right)^{0.41}$		34
53	$D + H^- \rightarrow H + D^-$	$k_{53} = 6.4 \times 10^{-9} \left(\frac{T}{300}\right)^{0.41}$		34
54	$D + H^- \rightarrow HD + e^-$	$k_{54} = 0.5 k_2$		35
55	$H + D^- \rightarrow HD + e^-$	$k_{55} = 0.5 k_2$		35
56	$D + D^- \rightarrow D_2 + e^-$	$k_{56} = k_2$		25
57	$HD + e^- \rightarrow H + D^-$	$k_{57} = 1.35 \times 10^{-9} T^{-1.27} \exp\left(-\frac{43\,000}{T}\right)$		36
58	$HD + e^- \rightarrow D + H^-$	$k_{58} = 1.35 \times 10^{-9} T^{-1.27} \exp\left(-\frac{43\,000}{T}\right)$		36
59	$D_2 + e^- \rightarrow D + D^-$	$k_{59} = 6.7 \times 10^{-11} T^{-1.27} \exp\left(-\frac{43\,000}{T}\right)$		36
60	$H^+ + D^- \rightarrow HD^+ + e^-$	$k_{60} = 1.1 \times 10^{-9} \left(\frac{T}{300}\right)^{-0.4}$		31
61	$D^+ + H^- \rightarrow HD^+ + e^-$	$k_{61} = 1.1 \times 10^{-9} \left(\frac{T}{300}\right)^{-0.4}$		31
62	$D^+ + D^- \rightarrow D_2^+ + e^-$	$k_{62} = 1.3 \times 10^{-9} \left(\frac{T}{300}\right)^{-0.4}$		31
63	$D^- + e^- \rightarrow D + e^- + e^-$	$k_{63} = k_{14}$		25
64	$D^- + H \rightarrow D + H + e^-$	$k_{64} = k_{15}$		25
65	$D^- + He \rightarrow D + He + e^-$	$k_{65} = 1.5 \times 10^{-17} T^2 \exp\left(-\frac{19\,870}{T}\right)$		31
66	$D^+ + H^- \rightarrow D + H$	$k_{66} = k_5$		25
67	$H^+ + D^- \rightarrow D + H$	$k_{67} = k_5$		25
68	$D^+ + D^- \rightarrow D + D$	$k_{68} = k_5$		25
69	$H_2^+ + D^- \rightarrow H_2 + D$	$k_{69} = 1.7 \times 10^{-7} \left(\frac{T}{300}\right)^{-0.5}$		31
70	$H_2^+ + D^- \rightarrow H + H + D$	$k_{70} = 1.7 \times 10^{-7} \left(\frac{T}{300}\right)^{-0.5}$		31

Table A1 – *continued*

No.	Reaction	Rate coefficient ($cm^3\ s^{-1}$)		Reference
71	$HD^+ + H^- \rightarrow HD + H$	$k_{71} = 1.5 \times 10^{-7} \left(\frac{T}{300}\right)^{-0.5}$		31
72	$HD^+ + H^- \rightarrow D + H + H$	$k_{72} = 1.5 \times 10^{-7} \left(\frac{T}{300}\right)^{-0.5}$		31
73	$HD^+ + D^- \rightarrow HD + D$	$k_{73} = 1.9 \times 10^{-7} \left(\frac{T}{300}\right)^{-0.5}$		31
74	$HD^+ + D^- \rightarrow D + H + D$	$k_{74} = 1.9 \times 10^{-7} \left(\frac{T}{300}\right)^{-0.5}$		31
75	$D_2^+ + H^- \rightarrow D_2 + H$	$k_{75} = 1.5 \times 10^{-7} \left(\frac{T}{300}\right)^{-0.5}$		31
76	$D_2^+ + H^- \rightarrow D + D + H$	$k_{76} = 1.5 \times 10^{-7} \left(\frac{T}{300}\right)^{-0.5}$		31
77	$D_2^+ + D^- \rightarrow D_2 + D$	$k_{77} = 2.0 \times 10^{-7} \left(\frac{T}{300}\right)^{-0.5}$		31
78	$D_2^+ + D^- \rightarrow D + D + D$	$k_{78} = 2.0 \times 10^{-7} \left(\frac{T}{300}\right)^{-0.5}$		31
79	$He^+ + D^- \rightarrow He + D$	$k_{79} = 3.03 \times 10^{-7} \left(\frac{T}{300}\right)^{-0.52} \exp\left(\frac{T}{22\,400}\right)$		31
80	$D + D^+ \rightarrow D_2^+ + \gamma$	$k_{80} = 1.9 \times 10^{-19} T_3^{1.8} \exp\left(\frac{20}{T}\right)$		31
81	$D + H_2^+ \rightarrow H_2 + D^+$	$k_{81} = k_4$		25
82	$H_2^+ + D \rightarrow HD + H^+$	$k_{82} = 1.0 \times 10^{-9}$		37
83	$HD^+ + H \rightarrow H_2 + D^+$	$k_{83} = 1.0 \times 10^{-9}$		37
84	$HD^+ + D \rightarrow D_2^+ + H$	$k_{84} = 1.0 \times 10^{-9}$		38
85	$HD^+ + D \rightarrow D_2 + H^+$	$k_{85} = 1.0 \times 10^{-9}$		37
86	$D + D_2^+ \rightarrow D_2 + D^+$	$k_{86} = k_4$		25
87	$H + D_2^+ \rightarrow D_2 + H^+$	$k_{87} = k_4$		25
88	$D_2^+ + H \rightarrow HD^+ + D$	$k_{88} = 1.0 \times 10^{-9} \exp\left(-\frac{472}{T}\right)$		38
89	$D_2^+ + H \rightarrow HD + D^+$	$k_{89} = 1.0 \times 10^{-9}$		37
90	$H_2 + D^+ \rightarrow H_2^+ + D$	$k_{90} = k_7$		25
91	$H_2 + D^+ \rightarrow HD^+ + H$	$k_{91} = \left[1.04 \times 10^{-9} + 9.52 \times 10^{-9} \left(\frac{T}{10\,000}\right) - 1.81 \times 10^{-9} \left(\frac{T}{10\,000}\right)^2\right] \exp\left(-\frac{21\,000}{T}\right)$		39
92	$HD + H^+ \rightarrow HD^+ + H$	$k_{92} = k_7$		25
93	$HD + H^+ \rightarrow H_2^+ + D$	$k_{93} = 1.0 \times 10^{-9} \exp\left(-\frac{21\,600}{T}\right)$		37
94	$HD + D^+ \rightarrow HD^+ + D$	$k_{94} = k_7$		25
95	$HD + D^+ \rightarrow D_2 + H^+$	$k_{95} = 1.0 \times 10^{-9}$		38
96	$HD + D^+ \rightarrow D_2^+ + H$	$k_{96} = \left[3.54 \times 10^{-9} + 7.50 \times 10^{-10} \left(\frac{T}{10\,000}\right) - 2.92 \times 10^{-10} \left(\frac{T}{10\,000}\right)^2\right] \exp\left(-\frac{21\,100}{T}\right)$		39
97	$D_2 + H^+ \rightarrow HD + D^+$	$k_{97} = 2.1 \times 10^{-9} \exp\left(-\frac{491}{T}\right)$		38
98	$D_2 + H^+ \rightarrow HD^+ + D$	$k_{98} = \left[5.18 \times 10^{-11} + 3.05 \times 10^{-9} \left(\frac{T}{10\,000}\right) - 5.42 \times 10^{-10} \left(\frac{T}{10\,000}\right)^2\right] \exp\left(-\frac{20\,100}{T}\right)$		39
99	$D_2 + H^+ \rightarrow D_2^+ + H$	$k_{99} = k_7$		25
100	$D_2 + D^+ \rightarrow D_2^+ + D$	$k_{100} = k_7$		25
101	$HD + He^+ \rightarrow HD^+ + He$	$k_{101} = k_{25}$		25
102	$HD + He^+ \rightarrow He + H^+ + D$	$k_{102} = 1.85 \times 10^{-14} \exp\left(\frac{35}{T}\right)$		35
103	$HD + He^+ \rightarrow He + H + D^+$	$k_{103} = 1.85 \times 10^{-14} \exp\left(\frac{35}{T}\right)$		35
104	$D_2 + He^+ \rightarrow D_2^+ + He$	$k_{104} = 2.5 \times 10^{-14}$		38
105	$D_2 + He^+ \rightarrow He + D^+ + D$	$k_{105} = 1.1 \times 10^{-13}\ T_3^{-0.24}$		38
106	$HD + D \rightarrow D_2 + H$	$k_{106} = 1.15 \times 10^{-11} \exp\left(-\frac{3220}{T}\right)$		30
107	$D_2 + H \rightarrow HD + D$	$k_{107} = \mathrm{dex}[-86.1558 + 4.539\,78 \log T + 33.5707\ (\log T)^2 - 13.0449\ (\log T)^3 + 1.220\,17\ (\log T)^4 + 0.048\,2453 (\log T)^5]$	$T \leqslant 2200\,\mathrm{K}$	28
		$= 2.67 \times 10^{-10} \exp\left(-\frac{5945}{T}\right)$	$T > 2200\,\mathrm{K}$	
108	$HD + H \rightarrow H + D + H$	See text		–
109	$HD + H_2 \rightarrow H + D + H_2$	See text		–
110	$HD + He \rightarrow H + D + He$	See text		–

Table A1 – *continued*

No.	Reaction	Rate coefficient ($cm^3\ s^{-1}$)		Reference
111	$HD + e^- \rightarrow H + D + e^-$	$k_{111} = 5.09 \times 10^{-9} T^{0.128} \exp\left(-\frac{103\,258}{T}\right)$	$v = 0$	40
		$= 1.04 \times 10^{-9} T^{0.218} \exp\left(-\frac{53\,070.7}{T}\right)$	LTE	
112	$D_2 + H \rightarrow D + D + H$	$k_{112} = k_9$		25
113	$D_2 + H_2 \rightarrow D + D + H_2$	$k_{113} = k_{10}$		25
114	$D_2 + He \rightarrow D + D + He$	$k_{114} = k_{11}$		25
115	$D_2 + e^- \rightarrow D + D + e^-$	$k_{115} = 8.24 \times 10^{-9} T^{0.126} \exp\left(-\frac{105\,388}{T}\right)$	$v = 0$	6
		$= 2.75 \times 10^{-9} T^{0.163} \exp\left(-\frac{53\,339.7}{T}\right)$	LTE	

Note: T and T_e are the gas temperature in units of K and eV, respectively. References are to the primary source of data for each reaction.
References: (1) Wishart (1979); (2) Ramaker & Peek (1976); (3) Karpas, Anicich & Huntress (1979); (4) Schneider et al. (1994); (5) Savin et al. (2004); (6) Trevisan & Tennyson (2002a); (7) Mac Low & Shull (1986); (8) Lepp & Shull (1983); (9) Martin, Keogh & Mandy (1998); (10) Shapiro & Kang (1987); (11) Dove et al. (1987); (12) Janev et al. (1987); (13) Ferland et al. (1992); (14) Poulaert et al. (1978); (15) Hummer & Storey (1998); (16) Aldrovandi & Pequignot (1973); (17) Dalgarno & Lepp (1987); (18) Schulz & Asundi (1967); (19) Barlow (1984); (20) Zygelman et al. (1989); (21) Kimura et al. (1993); (22) Peart & Hayton (1994); (23) Huq et al. (1982); (24) Walkauskas & Kaufman (1975); (25) same as corresponding H reaction; (26) Savin (2002); (27) Dickinson (2005); (28) fit to data from Mielke et al. (2003); (29) Gerlich (1982); (30) Shavitt (1959); (31) same as corresponding H reaction, but scaled by D reduced mass; (32) Stromhölm et al. (1995); (33) Linder, Janev & Botero (1995); (34) Dalgarno & McDowell (1956), scaled by D reduced mass; (35) same as corresponding H reaction, with branching ratio assumed uniform; (36) Xu & Fabrikant (2001); (37) estimate; (38) Walmsley et al. (2004); (39) fit based on cross-section from Wang & Stancil (2002); (40) Trevisan & Tennyson (2002b).

This paper has been typeset from a TEX/LATEX file prepared by the author.